Materials Horizons

ROYAL SOCIETY OF CHEMISTRY

REVIEW

View Article Online
View Journal

Cite this: DOI: 10.1039/d5mh00096c

Poly(3-hexylthiophene) as a versatile semiconducting polymer for cutting-edge bioelectronics

Ilaria Abdel Aziz, [a] Gabriele Tullii, [b] Maria Rosa Antognazza *[b] and Miryam Criado-Gonzalez *[ac]

Semiconducting polymers (SPs), widely used in organic optoelectronics, are gaining interest in bioelectronics owing to their intrinsic optical properties, conductivity, biocompatibility, flexibility, and chemical tunability. Among them, poly(3-hexylthiophene) (P3HT) has attracted great attention as a versatile SP, being both optically active and conductive, for the fabrication of smart materials (*e.g.*, films and nanoparticles), allowing the modulation of their performance and final biomedical applications. This review article provides an overview of the design of different kinds of P3HT-based materials, from chemical properties to structural engineering, to be used as key opto-electronic components in the development of opto-transducers for the modulation of cell fate, as well as biosensors such as organic electrochemical transistors (OECTs) and organic field effect transistors (OEFTs). Finally, their foremost applications in the biomedical field ranging from tissue engineering to biosensing will be discussed, including the future perspectives of P3HT derivatives towards cutting-edge applications for bioelectronics, in which optoceutics plays a key role.

Received 16th January 2025,
Accepted 15th April 2025

DOI: 10.1039/d5mh00096c

rsc.li/materials-horizons

Wider impact

Conjugated polymers are gaining increasing attention for the development of light-responsive materials offering promising potential for minimally invasive optoelectronic clinical therapies. This review article comprehensively compiles the works on the use of poly(3-hexylthiophene)-based materials in the emerging field of bioelectronics. Poly(3-hexylthiophene) (P3HT) stands out as the gold standard of p-type semiconducting polymers for (bio-opto)electronic applications due to its intrinsic sensitivity to visible light, biocompatibility, and cost-effective commercial availability, which has attracted the interest of many researchers worldwide. We focus on the development of innovative photo- and electro-active P3HT-based materials, which serve as efficient and highly biocompatible phototransducers, and discuss the perspectives of P3HT derivatives for cutting-edge bioelectronic applications. This review article presents original insights into fundamental, applied, and emerging research across materials science, nanoscience, polymer science, and bioelectronics, overcoming the limitations of traditional therapeutics through more efficient and biocompatible materials for the next generation of advanced optical and/or electrical therapies.

1. Introduction

Conjugated polymers (CPs), which have been widely used for decades in the electronic field (*i.e.*, organic photovoltaics, organic light-emitting diodes and organic field-effect transistors),[1,2] have recently attracted increasing interest in bioelectronics.[3,4] Beyond their intrinsic conductivity and optical properties, conjugated polymers offer chemical versatility, biocompatibility, and flexibility, making them excellent candidates for enabling the multifunctional properties needed at cell–material interfaces, particularly for the control of localized photoelectrochemical reactions.[5,6] The mechanism behind the optoelectronic properties of CPs lies in their extended conjugated molecular skeleton. The carbon atoms are in sp^2 hybridization state; hence the molecular orbitals are distributed along the conjugation plane (xy π orbitals, σ orbitals) and perpendicular to the plane (z π orbital, or p_z). The p_z orbitals are extensively overlapped in the backbone, where the bonding π (lowest unoccupied molecular orbital, LUMO, conducting) and antibonding π^* (highest occupied molecular orbital, HOMO) bands originate, also referred to as conducting (CB) and valence (VB) bands, respectively. The electrons populating the p_z orbitals are highly delocalized in

[a] *POLYMAT, University of the Basque Country UPV/EHU, Joxe Mari Korta Center, Avda. Tolosa 72, 20018, Donostia-San Sebastián, Spain*
[b] *Center for Nano Science andTechnology@PoliMi, Istituto Italiano di Tecnologia, 20134 Milano, Italy. E-mail: mariarosa.antognazza@iit.it*
[c] *Institute of Polymer Science and Technology (ICTP-CSIC), 28006 Madrid, Spain. E-mail: mcriado@ictp.csic.es*

the formed band where the high transport property originates. Pristine CPs present an energy gap between the HOMO and the LUMO bands, and are hence identified as semiconductors. To achieve electrical conductivity, the electrons must be pushed to populate the LUMO band, where they are free to move throughout the chains. Electrons are promoted to the LUMO feeding the energy in the form of light or electrical stimulations. Among different types of semiconducting polymers (SPs), polythiophenes have been widely investigated for bioelectronics. They effectively reduce the electrical impedance when used as coatings of electrodes allowing a stable and permanent device–biological tissue connection.[7] The electronic conductivity of polythiophenes is usually quite low, and the polymer is doped by introducing states in the gap to improve it.[8] Doping introduces additional charges in the polymer, which provokes a perturbation of the lattice and charge order. The newly introduced charges will relax to a lower energetic state by interacting with the lattice, which induces deformation and the creation of a trap state for the charges: polarons. Polarons are lower energy states compared to the conduction band; hence for the same temperature, electrons have more states to jump to, increasing the conductivity. Additionally, being partially delocalized along the chains, they improve chain-to-chain electron movement, a process known as hopping. In CPs, the side chain usually enhances solubility and structural order. Indeed, side chains with oxygen atoms increase the solubility or the dispersibility in water, which is greatly attractive for the *in situ* and *in vivo* fabrication of bioelectronic devices. Poly(3,4-ethylenedioxythiophene) (PEDOT) has been widely employed in the development

Ilaria Abdel Aziz

Ilaria Abdel Aziz was awarded her PhD in Physics in 2020, for developing smart light triggered interfaces based on organic semiconductors for bioelectronics applications. Her postdoctoral research focused on applying organic conductor based drug delivery devices to plants, to study and boost the plant response during stressful events such as drought. Then, she was awarded a Marie Curie Postdoctoral Fellowship, focused on conducting polymers for bioelectronics and environmental applications, which is the focus of her current research interests.

Gabriele Tullii

Gabriele Tullii obtained his PhD in Physics from Politecnico di Milano in 2019. He then joined the National Research Council (CNR) as a postdoctoral fellow, working on the fabrication and morphological characterization of micro/nanopatterned polymer-based substrates for surface enhanced Raman spectroscopy (SERS) applications. He currently works as a postdoc researcher at Italian Institute of Technology. His research activity concerns the study of optical excitation of living cells, mediated by micro/nanosized conjugated polymer-based photo-transducers.

Maria Rosa Antognazza

Dr Maria Rosa Antognazza is a permanent researcher at the Center for Nano Science and Technology, IIT, Italy. Physicist by background, she holds internationally recognized expertise in bioelectronics, and in particular in organic biotechnology. She was among the pioneers in the field of photoceutics, by proposing the synergistic use of organic semiconductors and light stimulation in both neural and cardiac applications. In her research activity, she carried out extensive characterization of biohybrid interfaces by optical, electronic, photo-electrochemical, ion imaging and electrophysiology techniques. Her current research interests are focused on the development of devices for control of living cells' fate and metabolism.

Miryam Criado-Gonzalez

Dr Miryam Criado-Gonzalez is a Ramón y Cajal Assistant Researcher at the Institute of Polymer Science and Technology (CSIC), Spain. She leads the research line on smart polymer/peptide-based materials for biomedical applications. Her research interests include the synthesis of functional polymers and polypeptides, the study of their self-assembly, the formation of intelligent gels with electrical and optical properties, and their additive manufacturing through 3D/4D printing technologies for advanced applications in the biomedical field. She received the E-MRS Young Researcher Award in 2021, the Emakiker researcher position from POLYMAT in 2022, and the EPF Future Faculty and Researchers Award in 2025.

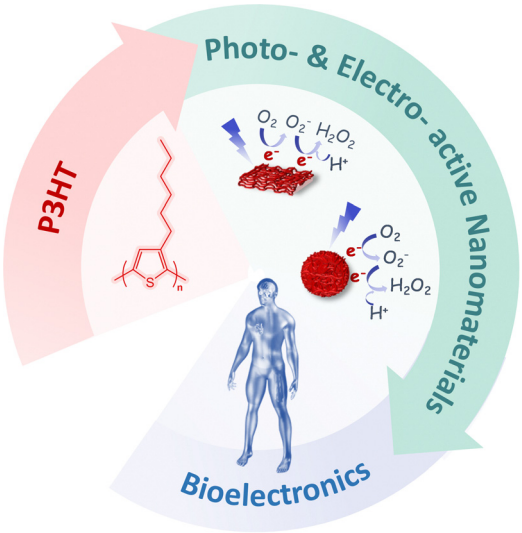

Fig. 1 Schematic representation of the employment of P3HT for the synthesis of photo- and electro-active nanomaterials to be used in bioelectronic applications.

of flexible and stretchable devices for bioelectronics due to its high conductivity, thermal stability and biocompatibility. Its mechanical and electrical properties can be tuned through the use of counterions, with polystyrene sulfonate (PSS) being the one that provides the best performance in terms of conductivity.[9–11] Nevertheless, PEDOT infusibility and insolubility limit its processability, and the material's efficiency is constrained by its carrier mobility being lower than that of poly(3-hexylthiophene) (P3HT) for optoelectronic-based biomedical applications.[12]

In this review article, we focus on the employment of poly(3-hexylthiophene) (P3HT), a p-type semiconducting polymer, for (bio-opto)electronic applications due to its biocompatibility, intrinsic sensitivity to visible light, and commercial availability at a competitive price. First, we will discuss the different strategies for doping P3HT and the photochemical properties. Then, we will focus on the employment of P3HT for the fabrication of photo- and electro-active nanomaterials (*e.g.*, films and nanoparticles) to be used as efficient and highly biocompatible phototransducers at bio-hybrid interfaces. We will also provide insights into the application of P3HT-based nanomaterials in bioelectronics, including tissue engineering, neuromodulation, and biosensing. Finally, the perspectives of P3HT derivatives toward cutting-edge applications in bioelectronics will also be addressed (Fig. 1).

2. Poly(3-hexylthiophene)

Poly-3-hexylthiophene (P3HT) is among the most widely studied p-type polymer for organic solar cells, field effect transistors and other electronic components. More recently, it became the workhorse polymer for light mediated stimulation of biological tissues and cells in bioelectronics. The monomer, 3-hexylthiophene (3HT), bears a thiophene ring with a hexyl alkyl chain, helping its solubilisation in organic solvents. The synthesis of P3HT can be performed through different chemical polymerization mechanisms: (i) the direct arylation protocol (DArP), which shows 95% regioregularity, (ii) the Grignard metathesis (GRIM) polymerization or other palladium-based catalyst polymerization approaches for dopant-free, which leads to a very high molecular weight, semiconducting and full regioregular polymers, and (iii) the established chemical oxidative polymerization of 3HT involving a strong Lewis acid as the oxidant (*e.g.*, $FeCl_3$), which can dope P3HT resulting in conductive rather than semiconducting polymers with different molecular weights.[13] P3HT can also be synthesized by electrochemical polymerization, giving a highly crystalline material directly formed on a conductive electrode. The P3HT polymer exhibits both regioregular (rr-) and regiorandom (rra-) periodicities. In the first case, the hexyl chains are regularly alternating between the positions 3 and 4 of the thiophene ring along the polymerizing chain, while in the second case the hexyl chain is randomly accommodated. In the regioregular case, the actual regioregularity extends for a certain number of repeating units, high enough to obtain extended crystalline regions where the thiophene rings are stacked in lamellar and interdigitated structures. Such structures have highly overlapped pi-orbitals, which are responsible for electron transport. In order to further increase the electronic conductivity, chemical and electrochemical doping have been deeply investigated. Indeed, doping in organic solvents with salts such as *tert*-butyl ammonium perchlorate or 2,3,5,6-tetrafluoro-7,7,8,8-tetracyanoquinodimethane (F4TCNQ) increased the electronic conductivity up to a few orders of magnitude in comparison with pristine films, either during electrochemical doping or by doping a spin-cast film.[14–16] However, dopant insertion in the polymer structure affects the mechanical properties. Recent studies reported on such interaction at the nanoscale.[17,18] Dopants preferably accumulated in crystalline regions of the polymer, reducing its Young's modulus, while amorphous regions were not affected by the presence of dopants.[17] Additionally, the higher currents were still recorded from the crystalline regions, where the dopants possibly foster electron transfer despite increasing the lamellar distance and reducing the crystallinity. A positive correlation was found between ion concentration and spectroelectrochemical measurements when P3HT is in contact with water-based electrolytes.[19] Further studies reported on different localization of the dopants depending on the electron affinity of the dopant itself: while molecules with low electron affinity localize in the crystalline regions, stronger oxidants affect both crystalline and amorphous regions.[20] Increasing the negative polarization of the polymer with respect to the open circuit voltage promoted the doping from the solution, resulting in higher absorption changes for higher electrolyte concentrations. Additionally, ions were mostly accumulated in amorphous regions, while crystalline regions were not strongly affected. Indeed, changes up to 11% in lamellar distance were also recorded for electrochemical doping of P3HT in ionic liquids or polymeric ionic liquids as electrolytes.[21]

P3HT is characterized by a wide optical absorption spectrum in the visible range. Upon photoexcitation, electrons are

promoted to the LUMO, leaving a vacant positive charge in the HOMO (hole), forming excitons. Electrons and holes diffuse in the polymer bulk, generating a capacitive charging of the surface (photocapacitive effect). The charges can be extracted (acceptor molecules and faradaic reactions or extraction layers) or recombine, generating heat (photothermal effect). By comparing the energetic levels of the semiconductor bands (LUMO −3.5/−3.2 eV *vs.* vacuum and HOMO −5/−5.5 eV *vs.* vacuum) with the redox potential of species such as oxygen, water, superoxide and salts, a little energy difference can be identified especially between molecular oxygen and P3HT LUMO (Fig. 2).[22,23] P3HT has been extensively studied for its photocatalytic activity related to reduction of molecular oxygen in water, as the reduction potential falls in the energy gap of the polymer (photoelectrochemical effect). The reduction of molecular oxygen generates superoxide radicals, which are unstable radicals, which together with the other successive reduction states of oxygen are collectively called reactive oxygen species (ROS), a class of strongly oxidative molecules. ROS are important secondary messengers in cellular metabolism and signalling, for both mammals and plants. Cellular redox balance, or homeostasis, refers to the equilibrium between oxidizing and reducing agents that is maintained within the cell in a healthy status. This equilibrium is mediated by multiple reactive species, in which ROS have been mostly identified as the pivotal mediator. The role played by ROS in pathophysiology appears very complex, and is strictly dependent on their intracellular concentration. ROS net balance results from the activity of numerous proteins and molecular processes within cells, which work as either ROS sources or ROS scavengers. This balance between ROS and antioxidants may have a double-edged impact on the different pathophysiological conditions. In fact, sufficiently "small" alterations of redox homeostasis can lead to a hormetic response, due to the activation of redox-sensitive pathways stimulating cell proliferation, growth, differentiation, and angiogenesis. On the other hand, oxidative distress can be induced and employed to trigger cell death.[24] It was demonstrated that P3HT was able to generate hydrogen peroxide (H_2O_2), a kind of ROS, upon illumination.[25] The H_2O_2 generation was restricted to the illuminated area and limited to the duration of irradiation, which enabled the spatio-temporal controlled generation of ROS.[22,26] This property has been studied for controlled ROS generation for bioelectronics,[27] reported in detail in Section 4.

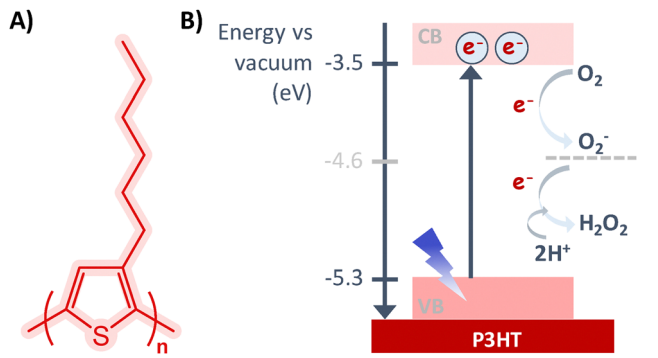

Fig. 2 (A) Chemical structure and (B) energy band gap of P3HT, including its photocatalytic activity to produce H_2O_2.

3. P3HT-based materials

This section reports on the design and development of P3HT-based materials, *ad hoc* engineered in the form of thin films and nanoparticles for bioelectronic applications.

3.1. P3HT thin films

Thin films (2D) of P3HT have been extensively studied in bioelectronics, especially for light-induced stimulation purposes, by interfacing them *in vitro* and *in vivo* with different cellular models[28–31] (*e.g.*, primary neuronal cells, astroglia cells, cardiac and endothelial cells)[32–40] and tissues (*e.g.*, explanted retinas and rat models for retinitis pigmentosa).[41–43] The fabrication protocol varied depending on the specific device architecture. Planar devices consisted of a sole P3HT layer or a multi-component structure in which the P3HT active layer was interfaced with conductive/semiconductive materials to enhance charge extraction. The simplest case was represented by the bare P3HT deposited on a rigid substrate, typically glass or glass/ITO. After thoroughly cleaning the substrate, P3HT solubilized in organic solvents was deposited on top by spin-coating (Fig. 3A and B). The thickness could be easily tuned, in the range of tens to hundreds of nm, by varying the deposition parameters (*e.g.*, material concentration, spinning velocity). P3HT exhibited a wide optical absorption spectrum in the visible range, with a maximum absorbance peak located around 520 nm (Fig. 3C), an important feature for photostimulation therapies, as will be discussed in Section 4. Considering that such films are supposed to be interfaced with cells and tissues, the material must fulfill three requirements: resilience to sterilization procedures, cell adhesion, and light-triggered properties in an aqueous environment. Surface treatment with adhesion proteins or extracellular matrix components (*e.g.*, fibronectin, poly-D-lysine) promotes cell adhesion to the material, otherwise hindered by the hydrophobic surface of the polymer film.[44] Alternatively, oxygen plasma treatment of the P3HT surface was proposed to enhance cellular adhesion by increasing the hydrophilicity of the polymer.[28,31,33,35,36,39,40] Concerning sterilization procedures, the typical protocols consisted of a thermal treatment by heating the films up to 120 °C for 2 hours, which additionally gave rise to thermal annealing that increased the crystallinity of the P3HT active layer.[28,31–33,35–37,39,40] In the case of heat-sensitive morphologies, the sterilization was carried out with 70% ethanol, an orthogonal solvent for P3HT.[27] In the case of *in vivo* studies, sterilization with gas (*e.g.*, ethylene oxide) was preferred.[41,43] On the other hand, for *in vivo* cases, the P3HT-based prosthesis is directly implanted in the animal models without any further modification.[34,43,45,46]

Cyclic voltammetry (CV) measurements (Fig. 3D) showed similar current densities between fibronectin-coated films,

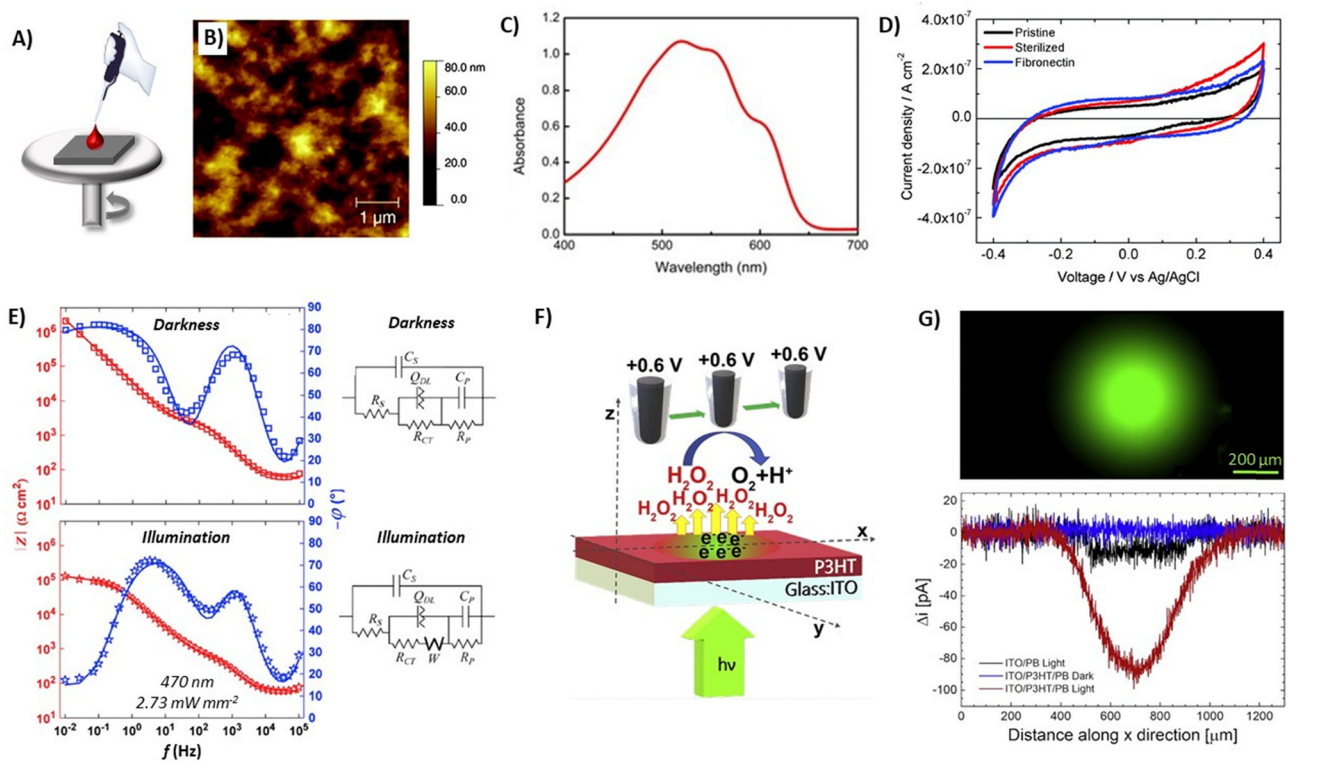

Fig. 3 (A) Schematic representation of the spin-coating methodology used to prepare P3HT thin films. (B) AFM topography image of a representative P3HT film. Reprinted with permission.[44] Copyright 2016 The Royal Society of Chemistry. (C) Optical absorption spectrum of P3HT thin films. Reprinted with permission.[31] Copyright 2017 Springer Nature. (D) Cyclic voltammetry at 100 mV s^{-1} of P3HT films. Reprinted with permission.[44] Copyright 2016 The Royal Society of Chemistry. (E) Bode plots of P3HT films deposited on ITO, in the dark and upon photoexcitation (λ = 470 nm, 2.73 mW mm^{-2}), including the equivalent circuits used to model experimental data. Reprinted with permission.[47] Elsevier B.V. (F) Schematic representation of the detection strategy of H_2O_2 production upon P3HT film photoexcitation, and (G) fluorescence image of the illuminated region of the film (top), and SECM scan lines of H_2O_2 production (bottom) measured as H_2O_2 oxidation current at the black platinum probe. Reprinted with permission.[27] Copyright 2020 Cell Press.

sterilized and pristine ones, thus indicating that the sterilization process and the fibronectin deposition did not affect the electrochemical properties.[44] The alternating current (AC) electrochemical behavior of ITO/P3HT devices was investigated by electrochemical impedance spectroscopy (EIS), both in the dark and upon illumination (Fig. 3E). The phase of the Bode plots at the open circuit potential (V_{eq}) in the dark (0.2 V *vs.* Ag/AgCl) and upon illumination (0.36 V *vs.* Ag/AgCl) showed three distinct regions: a minimum at high frequency (>10 kHz) and two maxima at intermediate (100 Hz–10 kHz) and low (<100 Hz) frequencies. The overall behavior at low frequency (<10 Hz) remarkably changes between dark and illuminated conditions: the illuminated devices presented a decrease of both the impedance modulus and the phase angle, ascribed to photo-oxidation reactions and electrolyte percolation through the polymer bulk.[47] Indeed, a sustained photofaradaic current was recorded during photo-stimulation (Fig. 3F), attributed to the reduction of molecular oxygen in the solution. In fact, the same photocurrent was suppressed in a nitrogen-controlled atmosphere. Oxygen reduction generated superoxide and hydrogen peroxide (H_2O_2) upon illumination,[25] with the generation confined to the illuminated area and limited to the irradiation time, as recorded by scanning electrochemical microscopy (Fig. 3F and G), which enabled the spatiotemporally controlled generation of ROS.[22,26]

A simple device based on a rigid substrate such as glass reduces the applicability *in vivo.* This drawback was overcome by using softer and more conformable materials (*e.g.*, polydimethylsiloxane (PDMS), polyethylene terephthalate (PET), and silk).[41–43,46] In those cases, the electrical contact could be provided by a thin film of organic and inorganic conductors deposited by spin coating prior to P3HT deposition. For example, Lanzani and co-workers deposited PEDOT:PSS on a silk substrate before P3HT deposition to adapt the device for retinal implantation.[42,43] The same group also proposed an alternative architecture, based on a PET substrate, coated with graphene for electrical contact and finally with P3HT for photoactuation.[41] The deposition of the graphene layer was carried out by chemical vapor deposition, prior to P3HT addition by spin coating. The standard bare P3HT architecture was also implemented by introducing n-type electron-accepting materials (*e.g.*, [6,6]-phenyl-C61-butyric acid methyl ester (PCBM) and the polymer poly{[*N*,*N*′-bis(2-octyldodecyl)-naphthalene-1,4,5,8-bis(dicarboximide)-2,6-diyl]-*alt*-5,5′-(2,2′-bithiophene)}(N2200)) interfaced with the polymer, leading to P3HT-based donor–acceptor thin films with a bulk heterojunction (BHJ) morphology for

bioelectronics purposes.[32,35,45,48] P3HT and the n-type material formed two interpenetrated domains with nano-scale morphology. It increased the efficiency of exciton dissociation and the transport of electrons and holes to the corresponding electrodes (*e.g.*, PEDOT:PSS, ITO) and the saline electrolyte. In the simplest case, the BHJ device architecture was usually obtained by preparing a mixture of P3HT and the electron-accepting material in the same solvent (usually at 1 : 1 ratio) and spin-casting the obtained solution on top of the desired substrate. A more complex architecture was proposed by Ghezzi and co-workers, which consisted of a foldable and photovoltaic wide-field epiretinal prosthesis.[46] The device was composed of a PDMS–photovoltaic interface, embedding 2215 stimulating pixels (active area: 12.7 mm) obtained through photolithography. Each pixel (80 and 130 μm in diameter) comprised a spin-cast PEDOT:PSS bottom anode, a P3HT:PCBM BHJ layer, and a top titanium (Ti) cathode. Another spin-cast PDMS layer encapsulated the device, protecting it from delamination and degradation. It has also been proven that P3HT electrochemical devices showed voltage-dependent heterogeneous swelling, which aligned with their operation and electrochromic behavior. Polymer semiconductors could function under both field-effect and electrochemical regimes simultaneously, depending on the nanoscale film morphology, ion concentration, and potential.[19] Recently, Lin and co-workers synthesized three types of P3HT-based block copolymers (BCPs) incorporating different insulating blocks (poly(*n*-butyl acrylate) (PBA), polystyrene, and poly(ethylene oxide) (PEO)) for application in organic electrochemical transistors (OECTs). P3HT-*b*-PBA copolymers demonstrated superior performance in a KCl-based aqueous electrolyte, with a higher mobility and capacitance than that of the P3HT homopolymer for OECT applications.[49] Peng *et al.* developed a stretchable OECT based on a 3D P3HT/styrene–ethylene–butylene–styrene (SEBS) porous elastic film capable of emulating biological synaptic behaviors for neuromorphic computing.[50] Ratcliff and co-workers designed floating gate OECTs for biological sensing. They used an ion gel with F_4TCNQ as the inert electrolyte for a P3HT channel accumulation mode transistor.[51] This kind of device was employed for the real-time monitoring of yeast (*Y. lipolytica*) in the working range of 10^3–10^6 CFU mL^{-1}.[52]

3.2. Physical and chemical strategies to modulate the properties of P3HT-based thin films

Living cells in the *in vivo* environment are embedded in the extracellular matrix (ECM), an intricate meshwork of glycosaminoglycans, proteins, and proteoglycans. The ECM parameters (*i.e.*, composition, concentration, and cross-linking grade of the structures) determine matrix stiffness and topography and are characterized by the presence of micro- and nanofeatures.[53] The interaction of the cell with this environment, mediated by the plasma membrane, is crucial in regulating cell homeostasis and function. The possibility to engineer conductive materials, such as conjugated polymers, to mimic the ECM–cell interaction is key for several promising applications, spanning from tissue engineering and regenerative medicine to neuroscience, and from pharmacology and physiology to neural computing.[53] The architectures developed to maximize the cell/device interaction can be divided into three main categories: planar, pseudo-3D and 3D. The topographical and chemical properties of the extracellular matrix (ECM) were mimicked by engineering surface roughness and through biofunctionalization. The increase of the device surface area is associated with different advantages: (i) a higher contact area effectively available to interface with cells, facilitating cellular adhesion; (ii) an enhanced electrical coupling, with reduced impedance and higher signal-to-noise ratio; and (iii) an increased efficiency towards electrochemical reactions. We developed P3HT-based photoactive micro-nanostructured planar devices by exploiting different all-solution processed fabrication routes. We designed a mesoporous indium tin oxide (ITO)/P3HT-based polymer/aqueous electrolyte interface by the subsequent deposition of ITO NPs and P3HT by spin coating, followed by thermal annealing steps. We demonstrated that mesoporous morphology affects the sign of the photo-generated charges accumulated at the device/electrolyte interface, changing the balance between capacitive and faradaic currents sustained by interfacial redox reactions. This effect was preserved also in the presence of the HEK-293 cell culture.[47] Micro- and nanopatterned polydimethylsiloxane (PDMS) molds were used for obtaining different 3D microstructures. A silk fibroin solution was drop-cast on top of micro- and nanopatterned PDMS molds, displaying the negative structure of three different topographies, nanostripes (∼800 nm width), small μ-wells (1–2 μm diameter), and big μ-wells (3.5 to 5 μm diameter). After solidification, the fibroin films were subjected to water vapor annealing to increase the silk crystallinity and make the films water-insoluble. P3HT was then deposited on the obtained silk films through spin coating by properly tuning the deposition parameters in order to avoid passivation of the surface topography. Notably, the P3HT layer displayed good homogeneity and the micro/nanostructured silk/P3HT films could hinder the adhesion of *Escherichia coli* up to 41% *vs.* flat control substrates.[54] In another work, we used a PDMS mold patterned with a microhole array of 2 μm diameter and 7 μm pitch between the centers of two adjacent holes. Then, a 1 μL drop of the P3HT solution in *o*-dichlorobenzene was pushed onto an ITO-glass substrate using the micropatterned PDMS mold and kept at 90 °C for 2 min. Subsequently, the mold was removed and a 4×5 mm^2 P3HT pillar array surrounded by a flat P3HT region was obtained (Fig. 4A and B). This micropatterned structure induced a remarkable change in the cell morphology of human embryonic kidney cells (HEK-293) and cortical neurons. Cells cultured on flat P3HT films presented a planar two-dimensional shape, while those cultured on the micropillars exhibited a more elongated cytoskeleton morphology.[55] Vurro *et al.* blended P3HT with high-density polyethylene (HDPE) to fabricate free-standing films with optoelectronic properties and customizable patterns by using a maskless laser ablation approach. These patterned films enabled the alignment of murine myoblast C2C12 cells to reproduce the structural complexity of living tissue.[56]

Chemical strategies to modulate the properties of P3HT films were also proposed. Recently, we synthesized graft copolymers,

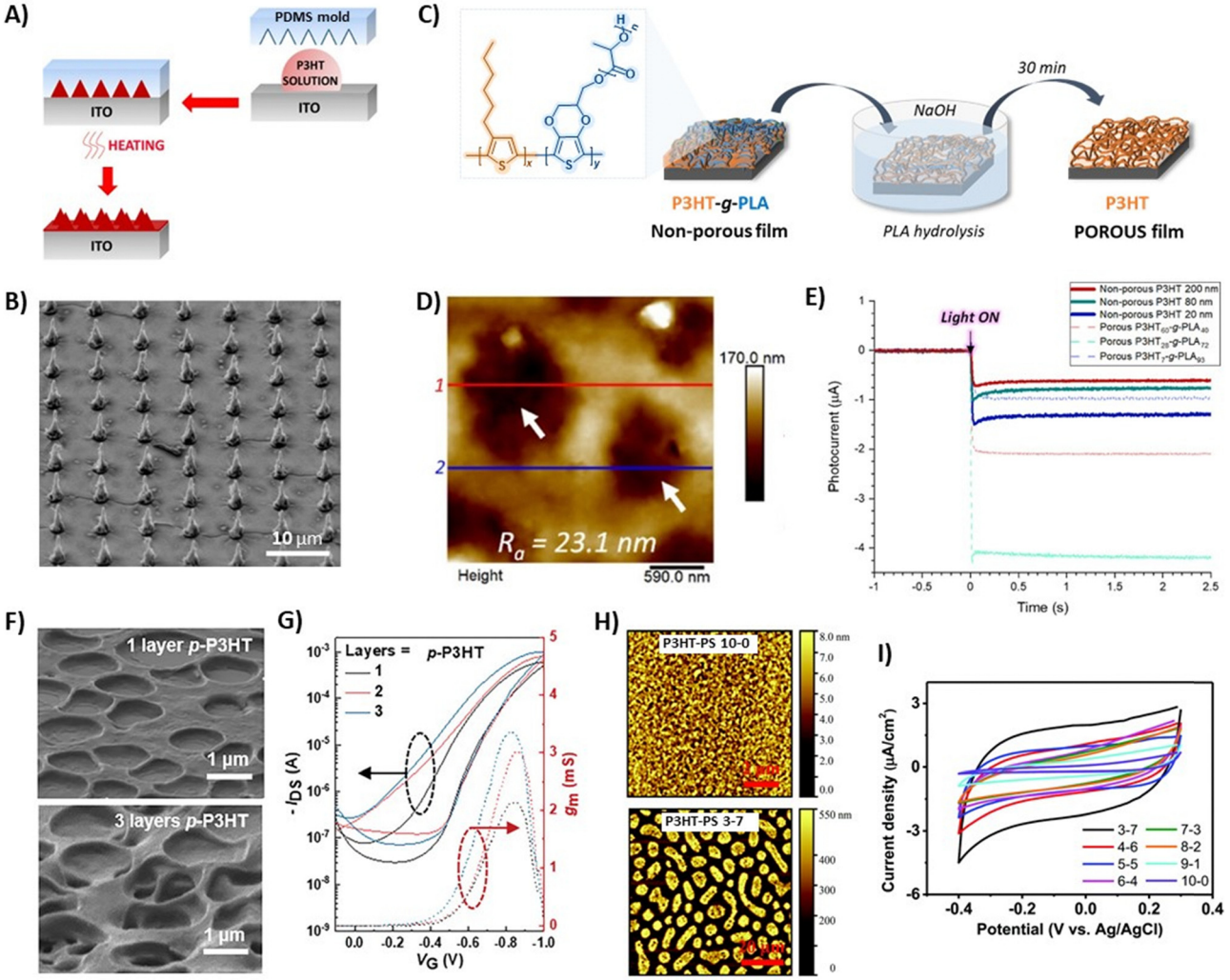

Fig. 4 (A) Schematic representation of the P3HT micropillar fabrication process by moulding, and (B) SEM image of P3HT pillar structure. Reprinted with permission.[55] Copyright 2019 American Chemical Society. (C) Schematic representation of the fabrication of porous thin films by PLA hydrolysis; (D) topographical AFM image of a representative porous P3HT film after PLA hydrolysis of $P3HT_{60}$-*g*-PLA_{40} copolymer film; and (E) photocurrent curves of non-porous P3HT films with different thicknesses and porous films made of $P3HT_x$-*g*-PLA_y copolymers when irradiated with a LED (530 nm, 110 mW cm^{-2}). Reprinted with permission.[57] Copyright 2023 American Chemical Society. (F) SEM images of porous P3HT/SEBS films, and (G) transfer curves and corresponding g_m evolutions for OECTs based on multilayers of P3HT. Reprinted with permission.[58] Copyright 2023 Wiley-VCH GmbH. (H) AFM images of porous P3HT films obtained from phase separation P3HT/PS followed by dissolution of PS by washing with acetone, and (I) CV scans (100 mV s^{-1}) of the O_2 plasma-treated porous P3HT films. Reprinted with permission.[59] Copyright 2020 The Royal Society of Chemistry.

made of P3HT and degradable poly(lactic acid) (PLA) segments, P3HT-*g*-PLA. Through hydrolysis of sacrificial PLA, nanometer-scale porous P3HT thin films were obtained. Pore sizes (220–1200 nm) were controlled by the copolymer composition and the structural arrangement of the copolymers during the film formation (Fig. 4C and D). The porous P3HT films showed an enhanced photofaradaic behavior, generating a higher photocurrent in comparison to non-porous P3HT films (Fig. 4E). With this strategy, we were able to modulate the intracellular ROS concentration in human umbilical vein endothelial cells (HUVECs) at non-toxic levels, thus affecting the physiological functions of cells.[57] Yu and co-workers combined physical and chemical strategies to develop porous P3HT/polystyrene-*block*-poly(ethylene-ran-butylene)-*block*-polystyrene (SEBS) films *via* constructing a multilayer breath-figured porous polymer channel (Fig. 4F). This elastic porous structure exhibited adjustable ionic–electronic coupling and transport pathways, while also offering resistance to mechanical tensile deformation. This porous structure was used as a porous channel in organic electrochemical transistors (OECTs), and provided an increase in transconductance (g_m) from 2.13 mS to 7.38 mS with the increase of deposited layers (from a single layer to a 3D layered structure) (Fig. 4G). The presence of SEBS conferred 60% mechanical stretchability with >21% g_m retained.[58] In another work, nanoporous P3HT films were obtained by dissolving polystyrene (PS) using acetone from previously formed films by spin-coating P3HT/PS mixtures at different ratios over ITO substrates (Fig. 4H). The nanoporous structure enhanced the

electrochemical capacitance, from 0.8 μF cm^{-2} (planar P3HT) up to 3 μF cm^{-2}, and the photocurrent, from 8 μA cm^{-2} (planar P3HT) up to 18 μA cm^{-2} (Fig. 4I).[59] As another example, nanostructured P3HT films were prepared by first coating gold (Au) substrates with P3HT (Au/P3HT) or with P3HT/poly(3,4-ethyldioxythiophene):poly(4-styrenesulfonate) (PEDOT:PSS) (Au/PEDOT:PSS/P3HT), and then applying cyclic potentials using cyclic voltammetry to produce interfaces with different surface roughness. The electrochemical impedance spectroscopy (EIS) measurements demonstrated that the nanostructured substrates significantly influenced the electrical and optical properties of P3HT at the interfaces.[60]

3.3. P3HT nanofibers

P3HT-based nanostructures of lower dimensionalities (1D) have also been developed. An all-solution processed approach was proposed by Yang *et al.* to develop P3HT nanoweb platforms to promote the neurogenesis of human fetal neural stem cells (hfNSCs).[61] They started from P3HT nanofibrils or nanorods formed by cooling (−20 °C) and heating (room temperature) cycles of a P3HT solution (*m*-xylene). The dispersion of P3HT nanofibrils and nanorods was then spin-coated on glass substrates. P3HT-based pseudo-3D substrates were also developed. Wu *et al.* developed micro/nanoscale structures of P3HT, which included nanofibers with an average diameter of 100 nm, microfibers with an average diameter of about 1 μm, and lithographically patterned stripes of 3, 25, and 50 μm width. Upon illumination, these P3HT structures provided electrical stimulation for neural differentiation and directed growth. Interestingly, neurons grown on P3HT nanofibers showed a higher number of branches, while those on P3HT microfibers exhibited longer and thinner neurites.[62] In another work, Jin *et al.* encapsulated P3HT in core–shell-structured gelatin/poly(L-lactic acid)-*co*-poly-(ε-caprolactone) nanofibers by coaxial spinning. Under light stimulation, the proliferation of fibroblasts improved compared to fibroblasts on the same scaffold under dark conditions. Lin *et al.* developed (P3HT)/poly(vinylidene fluoride-*co*-hexafluoropropylene) (PVDF-HFP) semiconductive nanofiber mat triboelectric nanogenerators (TENGs). The device exhibited an output power of 0.55 mW, which was enough to power 500 red light-emitting diodes and a digital watch. The P3HT-based nanofiber TENG could also be used as a sensor for monitoring human action.[63] Alimi and co-workers studied the confinement effect or nanostructuration effect on the photophysical properties of P3HT-based nanomaterials. To that aim, they fabricated nanofibers of ∼200 nm, which were made of a conjugated copolymer of P3HT and poly[2-methoxy-5-(2′-ethylhexyloxy)-1,4-phenylene vinylene] (MEHPPV). The molecular arrangement of MEHPPV-P3HT in the form of nanofibers increased the average exciton lifetime, which was twice as long in the nanofibers compared to the thin films.[64] The control of fiber formation allowed long-range alignment, which played a key role in charge carrier mobility. Deposition-based alignment methods, such as slide coating and blade coating, could further fine-tune fiber alignment, leading to long-range polymer chain alignment and resulting in field-effect mobility at the high end of what has been reported for P3HT.[65]

3.4. P3HT nanoparticles

Nanoparticles (0D) of organic semiconductors (NPs) are easier to synthesize and functionalize compared to inorganic nanoparticles. They can be obtained mainly through two methods: (i) a bottom-up approach that involves the direct polymerization of monomers in the dispersion media, and (ii) a top-down approach that consists of the dispersion of preformed oligomers or polymers in the medium.[66,67] The latter method is considered the most versatile to prepare water-suspended NPs and it was employed for the preparation of P3HT-based colloids for bioelectronics. A peculiar advantage of the top-down technique compared to direct polymerization is the possibility of creating nanoparticles made by a blend of different materials and controlling the composition ratio by varying the initial feed ratio of each material. Moreover, the possibility to modify the starting materials through easy synthetic routes allows for a wide property–function tuning of the energy gap, frontier orbital energies, optical properties, and charge transport characteristics.[68] The main methods to prepare P3HT NPs from the preformed polymer are nanoprecipitation and miniemulsion. In both cases, an organic solution of the material is injected into water, under magnetic stirring or ultrasound assistance (Fig. 5A). The formation of nanoparticles is allowed by the rapid change in solvent polarity which favours π–π stacking and hydrophobic interactions. However, the main difference in the two approaches is represented by the type of solvent: in miniemulsion, a water-immiscible organic solvent is employed, requiring the presence of surfactants to avoid coalescence of the emulsified droplets, whereas in nanoprecipitation the solvent is miscible with water and the NP dispersion can be surfactant-free. In general, nanoprecipitation yields smaller nanoparticles as compared to miniemulsion, down to a few nanometers. The experimental conditions (type of organic solvent, molecular weight and regioregularity of the polymer, starting material concentration, stirring speed, surfactant concentration, *etc.*) determine the size and the supramolecular organization within the NPs, which are in turn strongly related to the optoelectronic, charge transfer and charge transport properties. Surfactant-free P3HT NPs for biological applications were synthesized mostly through nanoprecipitation. The size obtained was in the range between 100 and 300 nm (Fig. 5B).[69] P3HT NPs also presented optical absorption in the visible range, with a maximum located at 520 nm, and fluorescence properties with a maximum emission peak centered at 650 nm (Fig. 5C). The photocurrent generation of P3HT NPs can be studied in a three-electrode configuration cell (Fig. 5D and E).[70] In analogy with previous results obtained with P3HT thin films, upon illumination, the oxygen reduction at the NP surface leads to the creation of ROS such as H_2O_2. The non-cytotoxic properties of P3HT NPs and their excellent uptake by cells made them ideal candidates for intracellular photo-stimulation therapies.

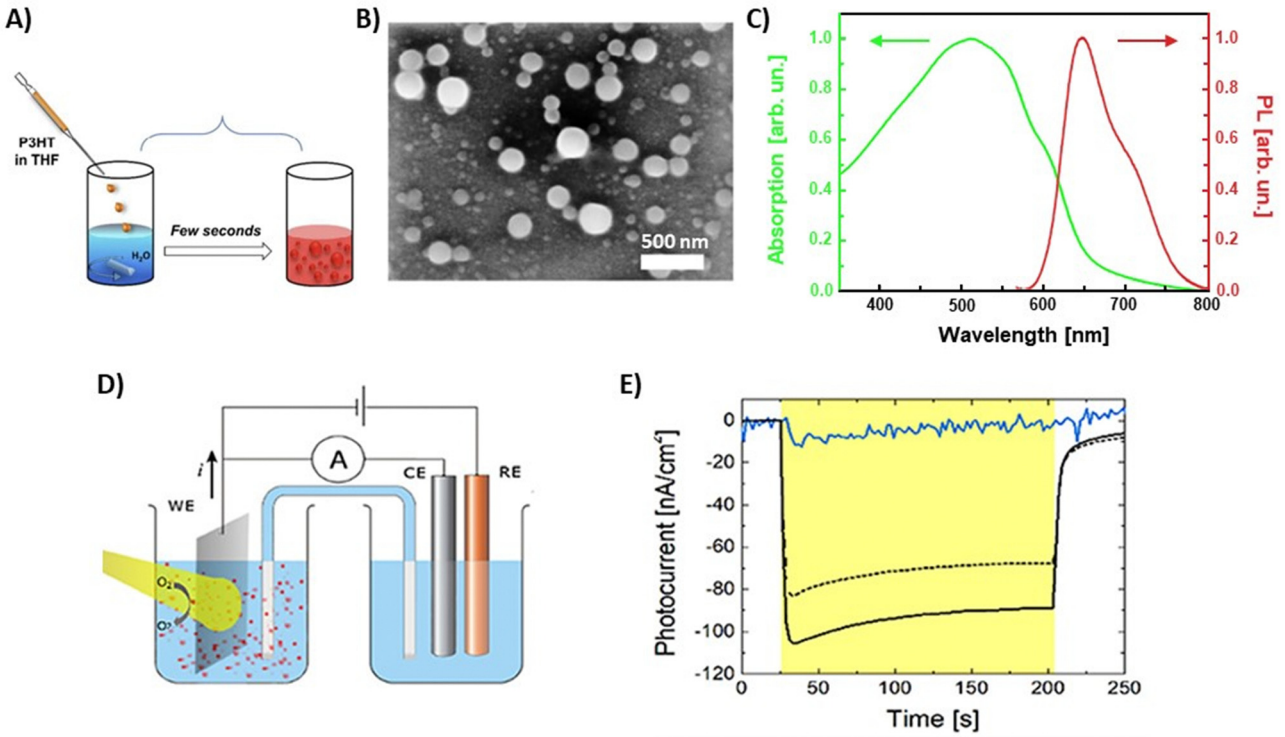

Fig. 5 (A) Schematic representation of the precipitation method used for the preparation of P3HT nanoparticles (NPs), and (B) representative SEM image of P3HT NPs. Reprinted with permission.[69] Copyright 2017 The Royal Society of Chemistry. (C) Optical absorption and fluorescence (PL) spectra of P3HT NPs in aqueous dispersion. (D) Experimental set-up used for photocurrent experiments and (E) Photocurrent spectra with and without molecular oxygen in solution at V = OCP−300 mV: ambient conditions with oxygen (black solid line), upon removal of oxygen in a nitrogen atmosphere (blue solid line), and upon partial re-oxygenation (black dashed line). The yellow shaded area represents the temporal window corresponding to optical excitation. Adapted and reprinted with permission.[70] Copyright 2018 Frontiers.

3.5. Physical and chemical strategies to modulate the properties of P3HT-based nanoparticles

In addition to bare P3HT nanosystems, P3HT-based nanoparticles with engineered surface morphologies and compositions were also developed. The surface properties and chemical composition strongly affect the stability, solubility, toxicity, and reactivity of the particles. Thus, the functionalization of organic NPs allows control of their interaction with biological systems, both *in vitro* and *in vivo*.[71] In general, the functionalization of polymeric NPs consists of the incorporation of specific moieties, such as chemically reactive groups (*e.g.*, amino and carboxylic groups, active esters), biologically relevant ligands (peptides, proteins, sugars) and/or electron-donor/accepting materials. This can be performed before (pre-assembly) or after (post-assembly) NP formation. In the pre-assembly approach, the functionalities are incorporated within the starting polymer either by encapsulation driven by electrostatic or hydrophobic interactions[72,73] or by direct conjugation through covalent bonding.[74,75] In the post-assembly approach, functionalities are attached to the surface of the formed NPs by covalent bonding (through chemical reactions)[68] or by non-covalent bonding (*e.g.*, hydrogen bonding, electrostatic or hydrophobic interactions).[76] These techniques allow obtaining different spatial distributions of the functional groups: in the pre-assembly case, the functional moieties are randomly distributed both inside and outside the NPs, while in the post-assembly case, they are confined in the outer layer without modifying the core of the NPs. Functionalized P3HT-based NPs for bioelectronics were developed by exploiting both assembly methods. The former was employed, for instance, to fabricate NPs bearing pendant *N*-succinimidyl-ester groups (NHS). To that aim, first, polythiophene derivatives with NHS at the terminal position of the side alkyl chains were synthesized and subsequently used to obtain nanoparticles by nanoprecipitation.[74] The presence of NHS led to the selective adhesion of the NPs to the plasma membrane of HEK-293 cells, in contrast to bare P3HT-NPs that are internalized within the cell cytosol. This property was attributed to the reaction between NHS and the primary amines of membrane proteins. A post-assembly approach was adopted by Di Maria *et al.* to functionalize a colloidal dispersion of P3HT NPs obtaining all-thiophene core–shell nanoparticles, characterized by the presence of a thiophene-based n-type material in the outer layer and P3HT in the inner core (P3HT@PTDO-NPs).[68] In particular, they showed that the treatment of P3HT NPs, obtained through nanoprecipitation, with Rozen's reagent ($HOF{\cdot}CH_3CN$) leads to the formation of a superficial layer containing thiophene *S*,*S*-dioxide (TDO) electron-accepting moieties. The presence of p-type (P3HT) and n-type (TDO) charge carriers in P3HT@PTDO-NPs allows for a stronger and longer-lived charge separation under illumination (Fig. 6A). This leads

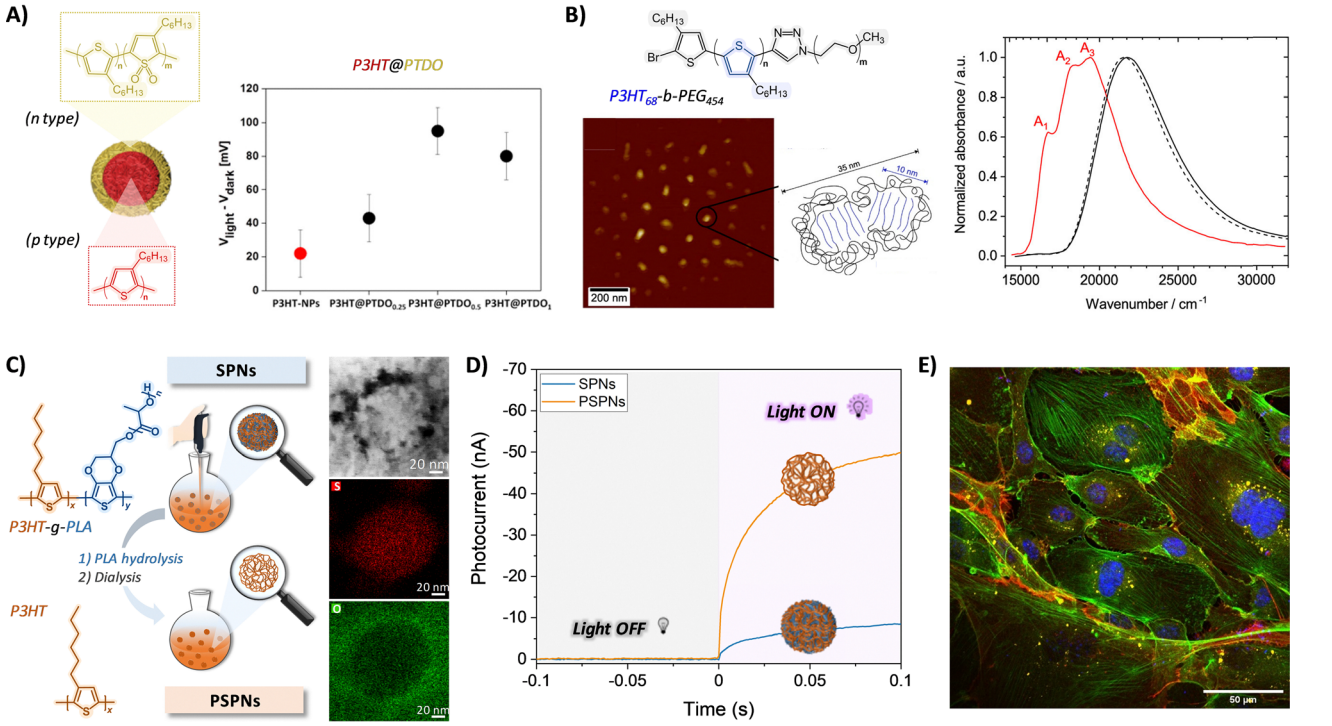

Fig. 6 (A) Schematic representation of the formation of core–shell P3HT@PTDO nanoparticles, and surface photovoltage values corresponding to different nanoparticles (red circle, P3HT-NPs; black circles, P3HT@PTDO-NPs). Reprinted with permission.[68] Copyright 2017, American Chemical Society. (B) Chemical structure of the P3HT-*b*-PEG block copolymer and AFM image of P3HT-*b*-PEG micelles formed in aqueous solution with an illustration of the aggregated P3HT core and the disordered PEG corona; UV/vis absorption spectra of the P3HT-*b*-PEG block copolymer and a P3HT homopolymer dissolved in the "good" solvent chloroform (black solid and dashed line), as well as of P3HT-*b*-PEG micelles in aqueous solution (red). Reprinted with permission.[78] Copyright 2021 American Chemical Society. (C) Schematic representation of the synthesis of P3HT porous nanoparticles (PSPNs) and TEM-EDX images of a representative PSPN. (D) Photocurrent curves of SPNs and PSPNs upon their irradiation with a LED (λ = 530 nm; 6 mW cm^{-2}). (E) Representative confocal fluorescence image of HUVECs treated with P3HT-PSPNs: nuclei (blue), actin filaments (green), CD31 (red), and PSPNs with intrinsic fluorescence represented in yellow for better visualization. Reprinted with permission.[79] Copyright 2024 American Chemical Society.

to improved photoelectrochemical activity which was exploited for the modulation of intracellular redox balance *in vitro* in HEK-293 line cells and *in vivo* in hydra polyps.[68,77] In another example, Beer *et al.* developed nanoscale aggregates by self-assembly of the block copolymer P3HT-*block*-poly(ethylene glycol) (P3HT-*b*-PEG) into micelles (~25 nm), with the P3HT aggregates constituting the micelles' core (Fig. 6B). The interplay between inter-aggregate, intra-aggregate, and intra-chain (structural and electronic) disorder within H-type P3HT aggregates, in combination with electronic interactions among polymer chains, ultimately determined their opto- and bio-electronic performance.[78] Very recently, we developed porous P3HT nanoparticles (PSPNs) with optimized photoelectrochemical efficiency, by following an approach that combines both pre- and post-assembly treatments. First, non-porous P3HT nanoparticles (SPNs) were synthesized by nanoprecipitation of a P3HT-*g*-PLA graft copolymer solution, coupled with the use of a biocompatible surfactant (Pluronic F-127) to stabilize the aqueous dispersion over time. Then, PSPNs were obtained by selective hydrolysis of the PLA pendants in the presence of a NaOH solution, followed by removal of byproducts through a dialysis step (Fig. 6C). PSPNs possessed a distorted round morphology (average diameter 58 ± 7 nm) with an enlarged surface area (54-fold increase in the surface area of PSPNs compared to non-porous SPNs). PSPNs exhibited an improved photoelectrochemical efficiency, corresponding to 4.5-fold increase in photocurrent associated with oxygen reduction reaction (Fig. 6D). This translated into >1.3-fold increase in the light-induced intracellular ROS production, tested in a well-established endothelial cell model, at a light density of a few mW cm^{-2} (Fig. 6E), fully compatible with *in vivo*, chronic applications.[79]

As in the case of thin films, the sterilization of the P3HT-based dispersions is crucial for safe and reliable employment in bioelectronics, in particular for *in vivo* studies. Methods to prepare sterile suspensions of P3HT-based NPs, without altering their physicochemical characteristics, are, therefore, strongly needed. In most of the *in vitro* and *in vivo* studies, sterile P3HT NPs are prepared through aseptic processing, *i.e.*, by employing sterilized water and laboratory glassware and conducting the whole process under a laminar flow hood.[69,70,74,80] However, aseptic processing presents two main drawbacks: (i) risk of microbial contamination due to several manual or mechanical manipulations of the sterilized product involved and (ii) the scaling of the method to production on an industrial scale is complex and costly. To overcome these problems, Monti *et al.* have developed an effective approach

to sterilize P3HT NP water dispersions based on the use of ionizing radiation.[81] They demonstrated that P3HT-NPs can be irradiated, either with γ-rays or with high-energy electrons (e-beam), under an inert atmosphere and with a dose up to 25 kGy, without affecting the physicochemical properties of the water dispersion, such as polydispersity, particle size, and aggregation, and ensuring long-term sterility (12 months). They observed that the selection of the proper dose rate is crucial for avoiding detrimental effects on the material: a high dose rate (kGy s^{-1}) preserves the characteristics of the polymeric NPs, while a lower dose rate (kGy h^{-1}) can damage the polymer. *In vitro* studies on human neuroblastoma SH-SY5Y cells demonstrated no cytotoxicity and a similar cellular uptake of P3HT NPs in all cases, regardless of the sterilization method employed, delivered dose, and dose rates.[81]

4. Applications of P3HT-based materials for bioelectronics

The chemical and physical properties typical of P3HT, together with endless possibilities to shape the material in different morphologies and its peculiar biocompatibility, paved the way for diverse applications in bioelectronics. The easy processability and the intrinsic electrical conductivity of P3HT were successfully employed in tissue engineering (Section 4.1). Distinct charge photogeneration and photocatalytic activity were at the base of several applications in the optical modulation of cells and tissues, as well as in the optical control of neurogenesis and cell fate (Section 4.2). Finally, the use of P3HT in biosensing was also successfully reported (Section 4.3).

4.1. Tissue engineering and regenerative medicine

P3HT is non-cytotoxic, but cells poorly adhere to its hydrophobic surface, which makes it necessary to apply protein-based coatings to enhance the cell adhesion properties for tissue engineering purposes. Scarpa *et al.* investigated the cell adhesion of L929 mouse fibroblasts derived from normal subcutaneous areolar and adipose tissue on P3HT films coated with fibronectin, collagen, and poly-L-lysine. The results showed that L929 cells attached and differentiated equally well on collagen and fibronectin coated films and more poorly on poly-L-lysine coated ones. Moreover, they also studied the effect of plasma surface oxidation to improve the surface wettability of P3HT films, which also enhanced their cell adhesion properties.

Although the electrical and conducting properties of the polymer were not affected by these treatments, the treatment with oxygen plasma could affect the P3HT phase.[29]

Sun *et al.* fabricated 3D tubular structures containing spatially distributed stripe patterns of P3HT and polylactic acid (PLA) on flexible polyimide (PI) films. These tubular P3HT-based structures provided a dual effect, as they first acted as contact cues to guide the growth and alignment of pre-osteoblasts and smooth muscle cells, and secondly, they were able to regulate the proliferation and osteogenic differentiation of pre-osteoblasts owing to the spatial electric signals of the P3HT conductive stripes.[82] Interestingly, this strategy could be useful for electrogenic (*i.e.*, bone, cardiac, and neural) tissue engineering applications. Concerning biocompatibility and biodegradability, electrospun scaffolds made of poly(lactide-*co*-glycolide) (PLGA)/P3HT blends were tested *in vivo* in a subcutaneous rat model. PLGA-undoped P3HT, PLGA-doped P3HT, and aligned PLGA-doped P3HT nanofibers were evaluated and compared with random PLGA fibers. All scaffolds, except PLGA-undoped P3HT, led to a decrease in inflammation over time. The aligned and PLGA-doped P3HT fibers initially triggered a moderate response at two weeks, which gradually diminished accompanied by a well-organized tissue structure and collagen deposition. These results demonstrated the biocompatibility and biodegradability of PLGA-P3HT nanofibers for tissue engineering purposes.[83] Zhenan Bao and co-workers went one step further to develop electronic skin (e-skin), defined as an artificial skin that mimics the properties of natural skin using electronic devices, for prosthetics, health monitoring, and smart soft robotics. They designed a bio-inspired stretchable e-skin with interactive color-changing, owing to the electrochromic properties of P3HT, and tactile-sensing properties. The device was integrated with a stretchable pressure sensor (PS), made of single-wall carbon nanotubes (SWNT) spray-coated over a polydimethylsiloxane (PDMS) dielectric layer, and a stretchable organic electrochromic device (ECD). This device was able to detect and distinguish varying pressure applied by means of a visible colour change in real-time, which made it very interesting for the development of colour-changeable e-skin.[84] In the field of e-skin, Park and co-workers designed a composite material comprised of a conductive layer, made of Li-complexed P3HT nanofibrils (Li-P3HT), and a stretchable layer, made of poly(styrene-*b*-butadiene-*b*-styrene) (SBS), as the active layers of the e-skin. High-performance strain and pulse sensors were obtained by printing Li-P3HT/SBS arrays on Ag nanowire/Ecoflex stretchable electrodes. The complexation of Li^+ and thiophene backbones increased the hole concentration of the nanocomposites, resulting in 5.7 times higher conductivity (1.27×10^{-3} S cm^{-1}) than that of pristine P3HT/SBS, while the stretchable SBS matrix allowed the retention of long electrical pathways *via* percolated Li-P3HT nanofibrils under up to 50% strain.[85]

4.2. Cell optical stimulation

One of the most distinctive features of P3HT is its intrinsic sensitivity to visible light, with a broad, optical absorption, between 400 nm and 600 nm, and a main absorption peak in the green spectral region, around 500 nm. Importantly, the P3HT optical absorption coefficient is remarkably high, in the order of $1–5 \times 10^{-5}$ cm^{-1} in the range of 400–600 nm, which is two orders of magnitude higher than that of silicon and about one order of magnitude higher than that of germanium or gallium arsenide.[86] This feature turns into the opportunity to fabricate thin, lightweight, flexible, and minimally invasive devices, in comparison with inorganic-based materials, whose lower absorption coefficient requires instead thicker active materials to get comparable sensitivity to visible light.

Additionally, visible light does not show toxic effects on living cells, compared for example to UV exposure. Therefore, it is not surprising that one of the major applications of P3HT in the organic bioelectronics field is mostly related to biophotonics and to the optical modulation of biological activity. Several *in vitro* and *in vivo* applications have been successfully reported in this context. While *in vitro* experiments on cell model systems allow for more in-depth analysis and quantitative understanding of photomodulation mechanisms, the actual processes operating under *in vivo* conditions often remain elusive, and a complete picture is in most cases replaced by semi-quantitative models, only partially verified by conclusive, killer experiments. Still, the huge work carried out by several groups in the latest years identified three main phototransduction processes, occurring at the interface between P3HT and its biological counterpart, namely, (a) photothermal, (b) photocapacitive, and (c) photoelectrochemical processes.[23,28,33,34,39,70,80,87]

In the first case, the light energy density absorbed by P3HT is rapidly converted into thermal energy, dissipated in the surrounding extracellular medium, which turns into modification of the cell membrane capacitance and/or into direct activation of temperature-sensitive channel proteins eventually expressed in the cell membrane of the considered model. In the photocapacitive mechanism, the light energy density absorbed by P3HT leads to the formation of charged states, which accumulate at the interface with the extracellular medium and establish a localized electric field. The latter, in turn, can modify the cell membrane equilibrium potential and lead to the elicitation of voltage-gated channels expressed on the cell membrane. In the photoelectrochemical process, the light energy density absorbed by P3HT leads to the formation of free charges, and in particular of free electrons which give rise to electron transfer processes and, owing to a favorable energetic alignment, subsequent reduction reactions of the oxygen dissolved within the extracellular medium. The photocatalytic formation of ROS in proximity to the cell membrane can trigger several different processes, including activation of pH-sensitive channels expressed on the cell membrane, modulation of the intracellular redox balance, activation of cell metabolic pathways and in some cases altered gene expression.

The above-mentioned processes are not mutually independent. They can occur in a competitive way (with one process prevailing over the others, within the same temporal range), simultaneously (with more than one process active at the same time), or in sequence (more than one process efficiently mediates phototransduction and modulation of the cell activity, but on different time scales). The prevalence of one mechanism over the others depends on several factors, including, to mention some non-exhaustive examples:

(i) The considered P3HT geometry (thin film *vs.* polymer fibers *vs.* nano- or microparticles). The physical dimensions and position (outside or inside the cell cytosol) of the active material can lead to a completely different outcome in terms of modulation of biological activity;

(ii) The P3HT morphology, as determined by polymer fabrication processes. This parameter determines key differences in the interaction with the cell model, in terms of cell seeding (*i.e.*, dimensions of the cleft), adhesion, and proliferation capability;

(iii) The light excitation protocol (energy density, duty cycle, repetition rate, wavelength, overall duration).

The above-mentioned factors are related to P3HT responsivity to optical stimulation. It is worth mentioning, however, that, while keeping all these conditions fixed, the most crucial factor determining the efficacy of the optical triggering remains the biological counterpart of the P3HT/biotic interface (*e.g.*, isolated *in vitro* cells, excised tissue, organs, *in vivo* settings). Even when considering a roughly simplified *in vitro*, bidimensional model composed of only one single cell type, it is necessary to take into account the huge differences between primary and immortalized cell lines (and related passage number), excitable and non-excitable cells, healthy and disease models, isolated cells and cell cultures at the confluence, among others. Depending on the mentioned conditions, the cell membrane equilibrium potential may vary around several tens of mV (*e.g.*, primary cardiomyocytes and glial cells, −90 mV; primary neurons, −70 mV; smooth muscle cells, −50 mV; endothelial cells, −40 mV, proliferating fibroblasts, −20 mV, tumor cells, −30 mV up to depolarized cell membrane positive potential of a few mV). Furthermore, in isolated cells, the interaction with the substrate is usually predominant, while for cells at the confluence, especially for those models able to create gap junctions, the cell-to-cell communication plays a major role in determining cell activity and response to external stimuli, being more significant than the interaction with the substrate. In addition, different cells are characterized by different morphologies, inherently related to their diverse functions, and this can imply a different value of the typical cleft dimensions, cell membrane capacitance, and expression of adhesion proteins. All these parameters have a sizable impact on the cell membrane's electrical and mechanical properties, turning into important differences in the relative weight of different phototransduction processes. Importantly, different cells express diverse temperature, voltage, strain sensitive ion channels, based on their different functions. ROS signaling pathways and intracellular redox balance significantly vary in diverse cell models, thus implying a markedly different sensitivity to modulation by exogenous, photoelectrochemically active materials.[24] Last but not least, some cells show remarkable, intrinsic responsivity to visible light, because they express in a more pronounced way light-sensitive proteins, like cytochrome *C*, involved in mitochondrial respiration and ATP production.[27] Several other conjugated polymers have been considered for cell photoactivation in the latest years, and we recommend to interested readers excellent recent reviews on this topic.[88–91] However, the P3HT/biotic interface remains a unique, prototypical system in which, owing to the collective work carried out by several research groups, a more in-depth understanding could be obtained, upon systematic variation of other parameters but the material type, and a semiquantitative model for photomodulation could be successfully derived.

In the following, we review some recent, remarkable results in optical modulation of cell activity by using P3HT, *in vitro* and *in vivo*, in which the predominant photostimulation protocol could be unambiguously identified or hypothesized based on experimental data and theoretical modeling. Successful examples of photomodulation of cell's electrical activity are first presented, in both electrogenic and non-electrogenic cells, followed by a more recent interesting application focusing on optical modulation of neurogenesis and neural development.

4.2.1. Optical modulation of electrical activity in electrogenic cells. In a pioneering work, Lanzani's and Benfenati's groups reported the use of regio-regular P3HT, employed as an electron donor, within a BHJ architecture with phenyl-C61-butyric acid methyl ester (PCBM) working as an electron acceptor. P3HT:PCBM thin films were deposited on top of transparent indium-tin oxide substrates and used as cell-seeding substrates for primary rat hippocampal neurons. Interestingly, green light stimulation of the photoactive semiconducting film triggered reliable action potential generation in neurons, with high spatial and temporal resolution and good reproducibility.[32] In these experiments, light intensity in the order of 15 mW mm^{-2} and stimulation frequency in the range of 1–20 Hz were used. On the other hand, Lanzani and co-workers used P3HT thin films as an interface with neurons to induce a light-mediated inhibition of their electrical activity in brain slices and explanted retinas for the *in vivo* modulation of neuronal activity. The prolonged irradiation of P3HT films (>500 ms), with visible or infrared light, caused hyperpolarization of the primary neurons' membrane due to a temperature-induced increase in the membrane capacitance, thus reducing spontaneous and electrically elicited action potential firings. These results introduced P3HT thin films as a new tool for the photo-inhibition of neuronal activity for treating pathologies related to neural hyperactivity, including epilepsy, or as retina prosthesis for the rescue of light sensitivity in retina degeneration.[33]

The most direct and ambitious application of optical modulation is indeed in the field of artificial vision, aiming at spatio-temporal fine-tuning of retinal ganglion cells. Based on the above-mentioned promising results, P3HT optoelectronic properties were largely exploited in the subsequent years to artificially mimic the green light responsivity of natural photoreceptors, rods in particular, and to rescue vision capability in blind retinas. P3HT thin films were used as photoactive substrates for both *ex vivo* experiments with explanted blind retinas and *in vivo* experiments in visually impaired rats. At first, degenerated retinal tissues in contact with P3HT thin films were measured *ex vivo*, and action potentials were reliably triggered upon stimulation with a light intensity of a few mW mm^{-2}.[34] A few years later, a layered, implantable device was realized by using silk fibroin as a biocompatible substrate, PEDOT:PSS as an ionically and electronically conductive interlayer and P3HT as a photoactive semiconductor sensitive to green light excitation. The devices were subretinally implanted in dystrophic rat retina models and they did not cause adverse gliotic or inflammation responses over several months.[42] Effective restoration of visual acuity was demonstrated, up to six months after implantation, by recording visually evoked potentials (VEPs), measuring the pupillary reflex, and assessing the animal behavior under dark and light conditions. Implanted devices were then explanted and characterized, and they were found to preserve the capability to generate charges upon photoexcitation while being relatively intact and undegraded.[34] Parallel works by other groups reported interesting architectures of retinal prosthetic devices for vision restoration, based on P3HT.[45] The group of K. S. Narayan demonstrated the use of a BHJ based on P3HT as an electron donor and naphthalene-based polymer N2200 as an electron acceptor, able to evoke neuronal activity in embryonic-stage blind chick retinal neurons, in an epiretinal configuration.[45] Evoked action potential characteristics correlated well with the optoelectronic properties of the polymer/electrolyte interface and resembled the natural response of the retina to light. However, the fraction of cells stimulated by the bulk heterojunction was around 10%, possibly due to the poor interface contact with retinal cells. A foldable, hemispherically shaped, minimally invasive array of organic photovoltaic cells based on P3HT coupled with microelectrodes of 130 mm diameter, called POLYRETINA, was realized by Ghezzi and colleagues.[46] The device embedded 2215 stimulating pixels, of which 967 were in the central area of 5 mm. Accelerated aging tests reported a lifetime of at least 2 years. In subsequent work, the authors opted for materials with optical absorption shifted towards the red spectral region, using different polymer blends;[92] *in vivo* results of POLYRETINA epiretinal implantation in Gottingen minipigs were first reported in 2022, showing light-evoked cortical responses in blind animals at safe irradiance levels.[93]

Despite encouraging results, the use of P3HT thin films or, more generally, polymer-based retinal implants for visual perception restoration puts some important constraints, since it requires complex surgical intervention for implantation, either in the epiretinal space or in the subretinal space. Thus, massive efforts have been made in order to develop light-sensitive nanoparticle colloidal dispersions, which can be injected and precisely delivered to the site of interest. In this case, the first successful results were obtained by using P3HT nanoparticles of about 300 nm diameter as the active and green light-sensitive material to endow inner retinal neurons with light sensitivity, while remaining in the extracellular space. When microinjected in the eye of dystrophic rats, P3HT NPs widely and persistently distribute in the whole subretinal space, in the absence of trophic effects on residual photoreceptors or substantial inflammatory reactions. P3HT NPs rescue light-driven behaviours, visual cortex activity, and visual acuity to levels indistinguishable from those of healthy congenic rats for up to 8 months after a single injection.[80] These results represented a milestone towards the possibility of developing an injectable, 'liquid' retina based on polymer nanoparticles,[94] and fostered a wealth of subsequent studies aimed, on the one hand, at understanding the mechanism behind *in vivo* functioning, and, on the other hand, at further optimizing P3HT as the election green-light sensitive material, given its largely proven

in vivo biocompatibility and photoelectrochemical stability. Regarding the first goal, a recent work by G. Chiaravalli showed an electrostatic coupling mechanism active at the biotic/abiotic interface as the most probable *in vivo* photoactivation mechanism.[87] Importantly, the photochemical mechanism, associated with the production of ROS, was disregarded, since it was expected to become relevant only at higher photoexcitation density, exceeding the physiological one. The importance of the presence of a highly resistive cleft, where ionic screening is negligibly small, was recognized here for the first time, to establish a significant pseudo-capacitive charging at the NP surface, responsible for electrostatic coupling. Under this condition, low physiological light intensities, in the order of 0.2 W m^{-2}, are able to induce appreciable depolarization of retinal neurons. In other words, the unavoidable protein corona and the establishment of a 'diffuse' interface are suggested here as the crucial element to ensure an effective coupling between retinal cells and P3HT NPs. Several types of water-soluble polythiophenes, particularly water dispersions of nanoparticles based on P3HT, have been synthesized, and recently reviewed.[95,96] For possible applications in artificial retina applications, core–shell nanoparticles composed of a P3HT core and a shell of its oxidized form PTDO have been synthesized by F. Di Maria and colleagues.[68] The nanosegregation of the two materials, in different regions of the nanoparticles, is expected to improve charge separation. Interestingly, P3HT@PTDO NPs present a different spatial localization of the excitation energy with respect to the non-oxidized NPs, showing a prevalence of surface states as a result of a different alignment of the HOMO/LUMO energy levels between the core and the shell. This feature was successfully employed to optimize the photostimulation of retinal neurons, as compared to P3HT-only NPs. Both NP populations were administered subretinally in degenerate retinas from the blind Royal College of Surgeons rats, and both were active in triggering light-induced retinal ganglion cell firing, but core@shell NPs displayed a significantly increased performance at both 7 and 18 mW mm^{-2}, indicating a higher sensitivity and more efficient energy conversion.

In summary, the use of P3HT as a photoactive material, in the form of either thin films or NPs, was demonstrated to be highly successful for neuromodulation applications, and in particular for endowing retinal ganglion cells with light sensitivity.[94] Noticeably, however, the approach successfully demonstrated for neurons revealed to be useful also for optical control of other excitable cells, namely cardiac and muscle cells. More recently, P3HT thin films were used as culturing substrates for human-induced pluripotent stem cell-derived cardiomyocytes. Reliable optical modulation of the contraction rate was successfully achieved, by using short (30 s) excitation pulses and photoexcitation densities in the order of 6–20 mW mm^{-2}.[36] In this case, at variance with the scenario elucidated in retinal implants, the phototrasnduction mechanism was identified in photothermal transduction, as largely documented by *ad hoc* control experiments. Whatever the mechanism behind stimulation, this work opened the way to the use of devices based on conjugated polymers for photomodulation, besides neurons, of excitable cardiac and muscle cells.

4.2.2. Optical modulation of physiological activity in non-electrogenic cells. Following the first successful reports of neuron culture control, the applications of P3HT soon extended well beyond stimulation of electrogenic cells, and a similar approach was explored to obtain reliable modulation of the activity of non-excitable cells and control of the passive electrical properties of their membrane. By definition, non-excitable cells are those cells that are unable to generate an action potential upon external stimuli: therefore, with the exception of neurons, muscle cells, and some endocrine cells, all cells in our body belong to this category. Here, cellular activity is mediated, rather than by rapid electrical signaling, by ion channels, which in turn activate slower intracellular biochemical responses. Several distinct types of voltage-gated and second-messenger-operated K^+, Ca^{2+}, Na^+, and Cl^- channels are present on the membrane of non-excitable cells, with specific functions in the regulation of the cell cycle, metabolic activity, and physiology. Such diverse channels represent an intriguing target for optical modulation triggered by P3HT. In particular, considering that biochemical processes occur on temporal scales much longer than electrical signaling (from hundreds of milliseconds up to hours and even days), intrinsically slower photothermal and photoelectrochemical transduction processes gain here more relevance as compared to fast photocapacitive charging.

At first, a very simple model of photoactivation triggered by P3HT thin films was derived by considering a secondary cell line, human embryonic kidney cells (HEK293).[28] Here, photothermal activation, with sizable modulation of HEK cell membrane resistance and capacitance, was unambiguously disentangled from purely photocapacitive charging effects. Subsequently, the possibility to reliably activate temperature-sensitive channels was reported in HEK-293 cells transfected with human transient receptor potential vanilloid 1 (TRPV1).[31] In general, TRPV channels have many fundamental roles in cell physiology, including body temperature regulation and chronic pain response. TRPV1 activation could be optically controlled with high spatiotemporal resolution, owing to a combined photothermal (localized temperature increase) and photoelectrochemical (localized pH variation in the extracellular medium) effect. Cell models of higher physiological relevance, as compared to HEK-293 models, which endogenously express temperature- and voltage-sensitive channels, were soon after considered, including astrocytes,[35] fibroblasts,[97] and endothelial cells.[39] Primary neocortical rat astrocytes were cultured on P3HT:PCBM thin films and the observed depolarization of astroglial cell membrane potential was attributed to modulation of the cell conductance and more specifically to modulation of ClC-2 chloride channel activity.[35] P3HT exposed to white LED light excitation showed an increase in fibroblast proliferation, as well as differentiation of adipose-derived stem cells toward epidermal stem cells, as compared to scaffolds without light stimulation or P3HT.[97] In endothelial cells, the TRPV1 channel plays a fundamental role in orchestrating vascular regeneration, thus representing a key pharmacological target for tissue repair in cardiovascular disease.[98] In 2019, F. Lodola

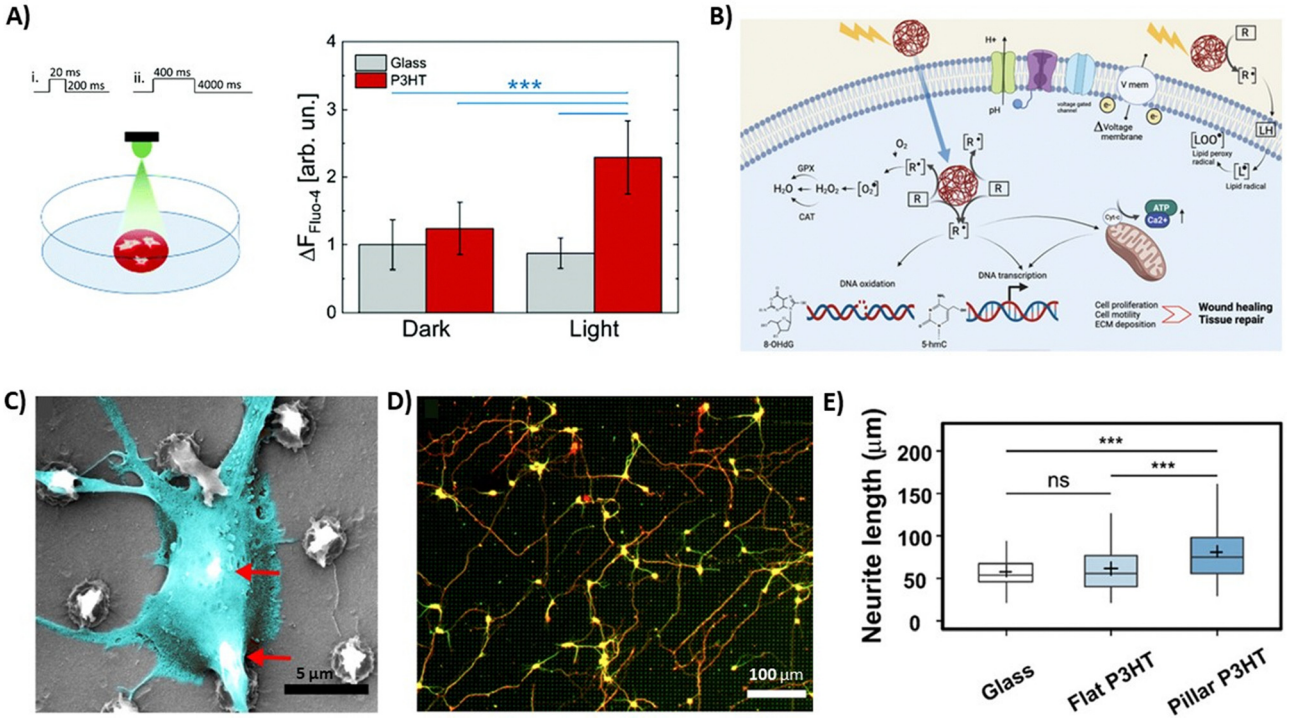

Fig. 7 (A) Sketch reporting the illumination conditions for the living cells in the home-made setup. The cells were illuminated from the top (400 μW mm^{-2}) with two different illumination patterns (left), and average variation of Ca^{2+} peaks under different experimental conditions is shown, after the 20/200 ms stimulation protocol. The statistical significance is reported for $p < 0.001$ (***), all other differences are not significantly different (right). Reprinted with permission.[100] Copyright 2022 The Royal Society of Chemistry. (B) Schematic representation of the biological pathways possibly induced by photostimulation of semiconducting polymer NPs. Reprinted with permission.[102] Copyright 2022 The Authors. Advanced Healthcare Materials published by Wiley-VCH GmbH. (C) SEM image of a neuronal soma suspended over two P3HT pillars. (D) Cortical neurons cultured on P3HT micropillars after 3 DIV, where neurons were fixed and fluorescently labeled for β-III-tubulin (green) and Tau-1 (red). (E) Average neurite length for 257 neurons on glass, 225 neurons on flat P3HT, and 229 neurons on pillar P3HT (data were compared using the non-parametric Mann–Whitney U-test with Bonferroni–Holm multiple comparison correction (0.05 significance level). ***$p < 0.001$, ns—not significant). Reprinted with permission.[103] Copyright 2021 American Chemical Society.

and colleagues reported a groundbreaking opportunity in the use of P3HT thin films for optical modulation of non-excitable cells.[39] They unambiguously demonstrated that human endothelial colony-forming cells cultured on top of P3HT thin films and exposed to visible light excitation during their first growth phases led to a robust enhancement of both proliferation and tubulogenesis. Interestingly, the mechanism mediating the effect was identified both at the cell level, through modulation of the Ca^{2+}-permeable transient receptor potential vanilloid 1 (TRPV1) channel, and at the molecular level, through downstream activation of the transcriptional factor NF-κB. The phototransduction process was unambiguously attributed here to the occurrence of photoelectrochemical processes at the P3HT surface, leading to spatially localized production of ROS species, all virtually ending up in an increase of H_2O_2 concentration and downstream elicitation of the TRPV1 ion channel.[40] This work represented a seminal proof of the principle of the possibility of using conjugated polymer photoexcitation to control the cell fate in progenitor cells, with a macroscopic outcome on cell proliferation and tubulogenesis efficiency.

The modulation of Ca^{2+} ion channels as a versatile tool to optically modulate the cell fate and the metabolic activity was also tested in other biological models.[99] As an example, intracellular calcium signaling triggered by P3HT photoexcitation was observed in human adipose-derived stem/stromal cells.[100] In this case, chronic exposure of cells cultured on top of P3HT thin films to visible light led to an increase in both cell responsivity and Ca^{2+} ion influx (Fig. 7A). A significant increase in the intracellular Ca^{2+} level upon periodic light stimulation was also reported by Ciocca *et al.*, in the case of neuroblastoma SH-SY5Y cells.[101] This effect was possibly attributed to the modulation of voltage-gated Ca^{2+} channels and/or to the activation of other Ca^{2+} permeable channels expressed on the cell membrane, as well as to the activation of intracellular Ca^{2+} storage compartments. Interestingly, photostimulation of cell/polymer interfaces was also accompanied by an inhibition of proliferation capability by about 50%, as compared to the cultures kept in the dark. However, while the reduced proliferation was not linked to an improvement in cellular differentiation, as demonstrated by the absence of expression of neuronal markers, it was also not related to cell reversible damage. Overall, polymer photoactivation mediated in this case a reversible alteration of the SH-SY5Y cell cycle. Interestingly, these results paved the way to use this approach not only for tissue regeneration, as reported by previously cited works, but also for tumour progression control and therapy.

Also in the case of non-excitable cells, *in vivo* translational opportunities can be maximized by the use of injectable, light-sensitive nanoparticles. Therefore, a lot of work has been carried out on P3HT nanoparticles in combination with secondary line cells, epithelial and endothelial cells, as well as with *in vivo* biological models, aiming at optical control of the cell fate. The first report showing modulation of Ca^{2+} trafficking by using P3HT NPs dates back to 2018.[70] In this work, Bossio *et al.* reported a sizable modulation of intracellular Ca^{2+} ion concentration upon internalization of P3HT NPs within HEK cells' cytosol. This was deterministically correlated to the P3HT NPs' photocatalytic activity and subsequent intracellular generation of reactive oxygen species (ROS) upon excitation, without affecting cell viability. This work, by first showing the capability of polymer NPs to produce ROS and to modulate Ca^{2+} dynamics by illumination on-demand, at non-toxic levels, opened the path to the use of polymer-mediated control of the cell redox state, under safe operational conditions, *i.e.*, without a detrimental effect on cell viability. A schematic representation of the process occurring within P3HT/keratinocyte interfaces after photostimulation was proposed by Antognazza, Tortiglione and coworkers (Fig. 7B).[102] In this case, human keratinocytes were used as an *in vitro* model to investigate skin repair. Data show that P3HT NPs delivered to cell cultures enhance both cell migration and proliferation capability and are rationalized based on the occurrence of photocatalytic processes and subsequent enhancement of intracellular ROS concentration at non-toxic levels. The effect of P3HT NPs on tissue regeneration capability was also tested *in vivo*, by using *Hydra vulgaris* as an ideal model for regenerative medicine.[104] Tortiglione's group showed that P3HT NPs' photoexcitation not only induces a behavioral and transcriptional change, by enhancing the animal contraction rate and opsin3-like gene expression, but, even more interestingly, also promotes faster tissue regeneration kinetics, enhanced stem cell proliferation, and change in the biomolecule oxidation levels by photoelectrochemical processes and P3HT photocatalytic activity.[102]

In general, redox balance modulation and ROS formation are now considered as the key mechanism for gaining optical modulation of the cell fate. From previously mentioned results, it is evident that the position of P3HT as an exogenous, ROS source material, either intra or extracellular, has a huge impact on the phototransduction mechanism.

4.2.3. Optical modulation of neurogenesis and neural development. The use of P3HT and optical excitation in synergy revealed to be successful also in the modulation of neurogenesis. One of the first studies dates back to 2016, when it was shown that an organic photovoltaic cell based on P3HT:PCBM in conjunction with an electrode for electrical stimulation enhanced neuron-like PC12 cell differentiation and neurite outgrowth, up to +64% as compared to control substrates, under NIR light illumination.[105] Later, Yang *et al.* self-assembled P3HT nanostructures (nanofibrils and nanorods) leading to nanoweb substrates to enhance the neurogenesis of human fetal neural stem cells (hfNSCs) *via* photo-induced electrical stimulation. The topographical morphology of the P3HT substrates in conjunction with the optoelectrical stimulation, *via* photochemical and charge-transfer reactions upon light irradiation (539 nm), activated the focal adhesion signaling of hfNSCs, and upregulated the expression and activation of voltage-gated ion channels in hfNSCs with the further increase of the neuronal differentiation of hfNSCs.[61] More recently, multiple efforts have been made in the attempt to realize a three-dimensional, photoactive scaffold for the control of neurogenesis, which can more closely resemble *in vivo* complexity. High aspect ratio P3HT micropillars were engineered as a mechanically compliant 3D platform to allow close contact with embryonic cortical neurons (Fig. 7C). Moreover, the combined action of nano/microtopography and visible light excitation induced the optical modulation of neuronal growth and orientation, with a significant increase in neurite and axon lengths (Fig. 7D and E). This platform enabled the optical modulation of neuronal growth in a wireless, repeatable, and spatiotemporally controlled manner without genetic modification.[103] A similar strategy was adopted by Colombo and co-workers, who performed the template-assisted electrochemical synthesis of P3HT nanowires doped with tetrabutylammonium hexafluorophosphate (TBAHFP) to obtain longer (*e.g.*, 17 $\pm$ 3 μm) or shorter (*e.g.*, 1.5 $\pm$ 0.4 μm) P3HT nanowires depending on the template employed. They showed that the nanowires were biocompatible and did not affect the electrophysiological properties of primary cortical neurons.[106] Wu *et al.* electro-span polycaprolactone (PCL)-P3HT microfibers and showed altered growth and differentiation of neuron-like PC-12 cells. In this compound, PCL provided a platform for supporting the P3HT function as a photovoltaic polymer. However, due to the inherent hydrophobic and non-polar functional group majority properties in PCL, this combination is not bio-friendly for cellular attachment. In a subsequent study, a fibrous platform made from PCL-P3HT and the biocompatible CP polypyrrole (PPy) was realized.[62] Interestingly, in the absence of the conducting polymer polypyrrole (PPy), the neurons showed a low cell survival due to increased intracellular reactive oxygen/nitrogen species production (ROS/NOs). When PPy was present in the membranes, it acted as an antioxidant and scavenged the ROs/NOs favoring the cell survival. It was found that such a structure has an optoelectrical conversion efficiency significantly better than that of PCL-P3HT and it wirelessly promotes PC-12 neurogenesis and growth/survival. The potential use of such a device as a cellular patch in optic and nerve regeneration was therefore proposed.[107] In another recent example, hydrophilic P3HT NPs were combined with an extracellular matrix-derived hydrogel matrix, thus creating a bioactive 3D platform.[108] When exposed to pulsed green light, P3HT NPs in hydrogels convert light signals into electrical signals, which in turn promoted the growth of cortical neurons and neuronal differentiation. Furthermore, it was demonstrated that P3HT NPs enhanced the expression of VGCC, thus elevating the influx of Ca^{2+} and activating the phosphorylation of PI3K/Akt and MEK/ERK biophysical pathways, finally resulting in neuronal differentiation.

4.3. Biosensing

P3HT can be employed for biosensing applications owing to the physical and/or chemical changes it undergoes when exposed to different analytes in gaseous or aqueous environments.

Furthermore, the molecular structure and morphology of P3HT-derived materials can be tailored through the incorporation of specific receptor sites, allowing for the fine-tuning of their chemical and physical properties, while simultaneously improving their sensitivity and selectivity. The confinement of proteins on a surface has garnered significant attention because of its importance in the development of biosensors for clinical applications. In this regard, Torsi and co-workers integrated biotin-binding proteins, including avidin (AV), streptavidin (SAV), and neutravidin (NAV), at the dielectric/organic semiconductor interface of two organic thin film transistors (OTFTs), to quantitatively analyze the processes that occur in protein–ligand complex formation and involve surface bound biological recognition elements. They integrated a functional bio-interlayer organic thin film transistor (FBI-OTFT) and a preformed complex organic thin film transistor (PFC-OTFT) so that the threshold voltage (V_T) was related to the protein dipole moment and the field-effect mobility (μ_{FET}) to the protein dipole moment when ligand binding occurred. The results showed significant V_T fractional changes only for the PFC-OTFTs upon exposure to biotin. On the other hand, fractional changes of μ_{FET} were observed only for the FBI-OTFT devices.[109] In another work, they developed smart organic field-effect transistors (OFETs), whose architecture was formed by a P3HT and streptavidin interlayer deposited on a SiO_2/Si substrate, for biotin sensing. They studied the influence of two different fabrication methods, spin-coating and dipping layer-by-layer (LbL) deposition, on the final performance of the OFETs. The LbL deposition led to a smoother and better-defined bioelectronic interface with part-per-trillion sensitivity to detect biotin.[110] Apart from that, they also developed a millimeter-wide electrolyte-gated field-effect transistor (EGOFET), which enabled label-free selective single-molecule detection of both genomic and protein biomarkers. With the aim of designing stable and cost-effective EGOFETs, the ink-jet printing technology was used for the fabrication of the P3HT channel, and compared with more commonly used spin-coating techniques. The device structure was formed by a coplanar lateral gate electrode and a FET channel with high control on their relative distance, which enabled mechanical and electrical stability (Fig. 8A and B). Interestingly, the ink-jet printed P3HT film exhibited a low energetic disorder (better π–π stacking in the crystalline regions), thus endowing OFETs with high performance in terms of stability and electronic performance for point-of-care (POC) sensing applications (Fig. 8C and D).[111] Another important issue in this field is the design of biosensors to detect cancer biomarkers. In this context, Elnagar *et al.* developed a biosensor for the detection of folate receptors (FRs). It was composed of folic acid, a biorecognition element to target FRs, which was conjugated to P3HT conducting nanofibers (CNFs), sodium alginate (ALG), and polyethylene oxide (PEO). The resulting biosensor possessed enhanced sensitivity, as it enabled the detection of FRs in human plasma with a limit of detection (LOD) of 0.12 pM, and improved selectivity. Therefore, it could be used as a theragnostic nanoprobe for early cancer diagnosis and treatment.[112] In another study, a composite membrane-modified carbon fiber (CFMEs) microelectrode was fabricated to detect ascorbic acid (AA). It was based on P3HT and nitrogen-doped multi-walled carbon nanotubes (N-MWCNTs) and presented good linearity,

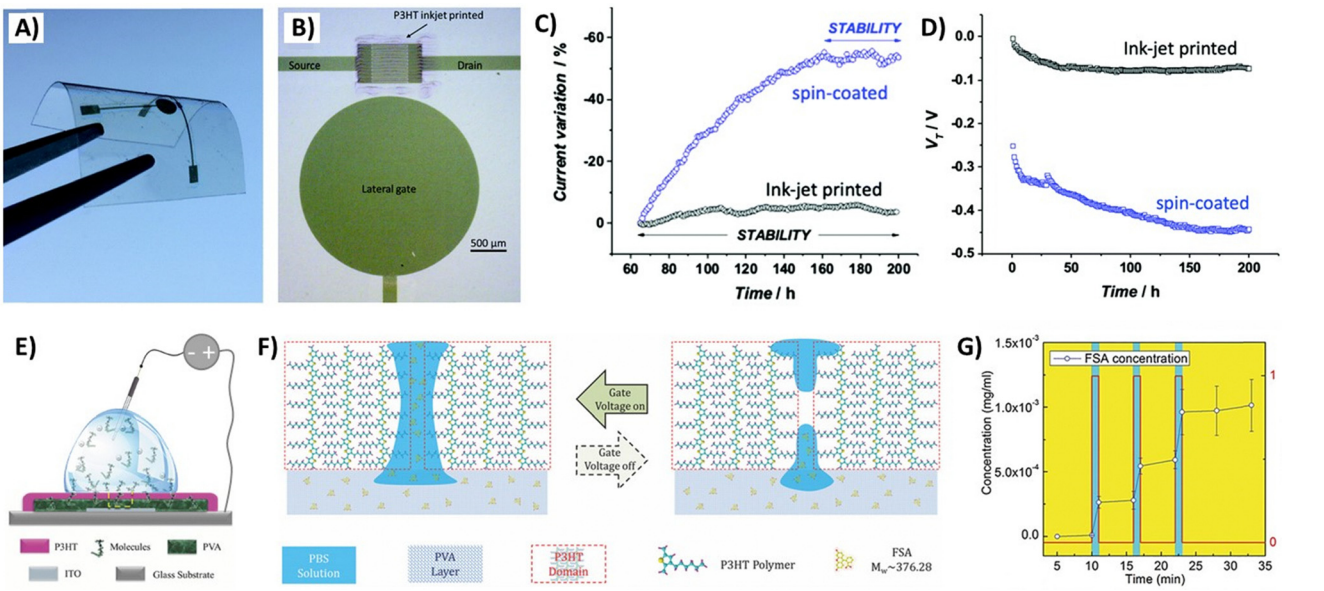

Fig. 8 (A) Optical microscope image of an EGOFET fabricated by ink-jet printing and standard photolithography; (B) picture of the device after a polystyrene cell is glued around the transistor channel; (C) percentage variation of $I_{D\,max}$ after the acquisition of the first 64 transfer curves till the 200th curve measured on an EGOFET comprising a spin-coated (blue circles) or an ink-jet printed (black circles) P3HT film; (D) P3HT based EGOFETs' threshold voltage (V_T). Reprinted with permission.[111] Copyright 2020 The Royal Society of Chemistry. (E) Schematic diagram of the device based on a P3HT/PVA/ITO multilayer and operated in an aqueous solution, with the Ag/AgCl electrode placed in the electrolyte; (F) schematic diagram for the voltage-controlled permeability and switchable molecule release of a P3HT film; and (G) the concentration of released FSA (left axis) as a function of time under the application of bias voltage (right axis). Reprinted with permission.[114] Copyright 2017 Wiley-VCH Verlag GmbH & Co.

selectivity, stability, and biocompatibility for neuroelectrochemical sensing. The microelectrode was further employed to monitor AA release from *in vitro* nerve cells, *ex vivo* brain slices, and *in vivo* living rat brains. The working principle was based on the activation of glutamate by the *N*-methyl-D-aspartic acid receptor, which enhanced the inflow of Na^+ and Cl^- ions to induce osmotic stress that caused cytotoxic edema and the AA release. Therefore, the P3HT-based microelectrode could be used for monitoring neurochemicals and the early detection of brain diseases.[113]

P3HT-based materials have also been employed for controlled drug delivery. As organic electronic ion pumps showed high operating voltages and limited transportation efficiency, Liu *et al.* designed an organic device based on P3HT for the low-voltage-controlled release of an anticancer drug to inhibit the growth of cancer cells by remote control. The device was formed by a multilayer structure built over on an ITO-glass electrode (Fig. 8E). A solid source electrolyte layer of polyvinyl alcohol (PVA) containing an anticancer drug (cisplatin) or fluorescein sodium salt (FSA) was first deposited over the ITO-glass. Then, a P3HT thin film was deposited on the PVA layer. The release of the drugs, stored in the source layer, was controlled by applying a voltage between the bottom electrode (ITO) under the PVA layer and the Ag/AgCl electrode in the target electrolyte. The drug release was possible due to the unique switchable permeability of P3HT in aqueous solutions under an applied bias voltage, which modulated its wettability through oxidation or reduction processes (Fig. 8F and G).[114]

4.4. Clinical trials involving P3HT-based materials

Most clinical trials performed until now have been focused on point-of-care (POC) applications to register physiological signals from patients. For example, Park and co-workers fabricated a wearable oxygen (O_2) sensor for transcutaneous O_2 pressure ($tcpO_2$) monitoring. It was formed by three layers integrated in a bandage-like configuration: a luminescent sensing film attached onto the skin by a carbon tape, an organic light-emitting diode (OLED) as a light source, and an organic photodiode (OPD) as a light detector. This sensor was placed on the lower arm and the thumb of a healthy volunteer, and, on the other side, a cuff and a ribbon were wrapped around the forearm and the thumb of the volunteer, respectively, to restrict the blood outflow. Then, the $tcpO_2$ variations were measured before, during, and after the occlusion, even when the person was exercising or working. The results pointed out a better performance of this sensor to register the $tcpO_2$ response on the thumb in comparison to the commercially available PeriFlux 5000, which could not measure the $tcpO_2$ on the thumb because it could not be stably in contact with the narrow area of the thumb tip.[115] Soppera and co-workers developed a sensor with a double active layer that exploited an ultrathin layer of P3HT, which served as a work function buffer to enhance the operational current while monitoring breath ammonia (BA) in hemodialysis (HD) patients. The results showed a good correlation coefficient of 0.96 between BA and blood urea nitrogen (BUN) levels.[116] Wang *et al.* designed a film-based sensor, which was made of P3HT/butyl rubber (BR), eutectic gallium-indium (E-GaIn), and polydimethylsiloxane-P3HT/BR, and used for electrocardiogram (ECG) monitoring. ECG signals from six healthy men and women volunteers were registered while they performed different activities such as meditation, leg exercising, weight lifting, fisting, and various hand gestures. The sensor possessed adhesive properties and successfully attached onto the wrists, ankles, and chest of volunteers, showing long-term durability and even underwater stability. The P wave, QRS complex, and T wave in ECG signals were identified, showing no significant difference in ECG monitoring performance with a commercial gel electrode, thus providing valuable medical information for clinical use.[117] On the other hand, in the case of neurostimulation therapies using P3HT nanoparticles, the clinical translation remains limited. A key step in this clinical translation process is the control of fate and harmfulness of P3HT nanoparticles *in vivo*. They must be tailored to target specific neuronal subpopulations and, potentially, be able to cross the blood–brain barrier to reach the brain following peripheral administration.[118]

5. Perspectives of P3HT derivatives towards advanced applications

P3HT-based implantable devices have shown promising results in different biomedical fields, where improvements for specific targets focused both on the material *per se* and on the

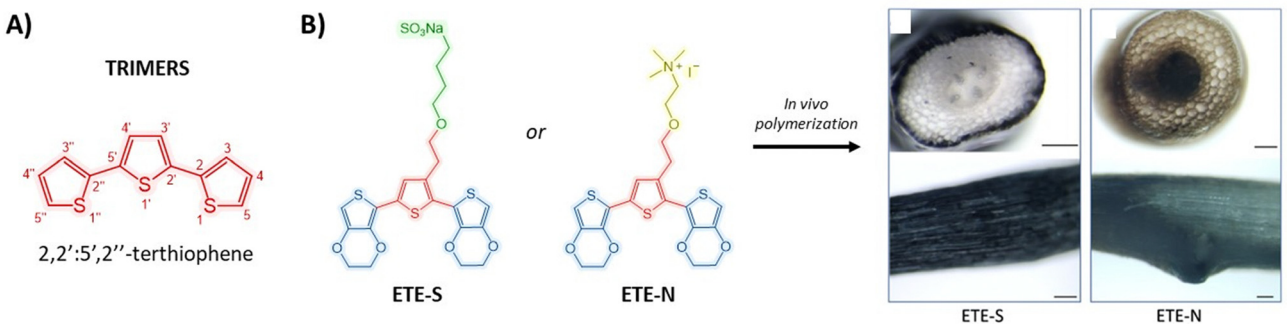

Fig. 9 (A) Chemical structure of terthiophene (thiophene trimer). (B) Chemical structures of ETE-N and ETE-S trimers polymerized *in vivo* along the roots of living plants due to the presence of native peroxidase enzymes, and cross-sectional (top) and lateral views (bottom) of the bean roots (scale bar = 100 μm). Adapted and reprinted with permission.[126] Copyright 2020 American Chemical Society.

substrate, for example employing flexible ones. However, P3HT is a rather hard polymer, with a Young's modulus in the order of GPa.[119] As biological tissues' Young's modulus is in the 10–1000 kPa range, a mechanical mismatch arises at the interface between the polymer and cells or tissues. Only recently, some studies started to correlate local ion intercalation with changes in the mechanical properties of P3HT, mostly limited by the hydrophobic nature of the polymer.[119] Extending our considerations to polythiophene derivatives, the possibility to change the mechanical properties on demand has been achieved mostly through composites, while synthetic approaches have been exploited only to a small extent. Recently, a

Table 1 Summary of the main types of P3HT-based materials and light excitation conditions used for (bio-opto)electronic applications

		Light excitation conditions					
Material type	Material form	Wavelength (nm)	Intensity (mW mm^{-2})	Time	Biological models	Biomedical applications	Ref.
P3HT	Thin films	544	26–344.57	100 ms	HEK-293 cells	Photo-stimulation of the TRPV1 channel	31
P3HT	Thin films	532	4–15	10–100 ms	Hippocampal neurons, retinas explanted from albino rats	Visual restoration	34
P3HT	Thin films	525	0.4	30 ms	ECFCs	Proliferation and tubulogenesis	39
P3HT	Thin films	544	0.6	2.5–20 s	ECFCs	Photo-activation of TRPV1-mediated intracellular Ca^{2+} signals	40
P3HT	Thin films	550	4–20.2	30 s	hiPSCs	Tissue engineering	36
P3HT	Thin films	530	1.1	180 s	HUVECs	ROS modulation in vascular tissue	130
P3HT	Thin films	525	0.2	20–400 ms	hASC cells	Regenerative medicine	100
P3HT	Thin films	530	0.0126	1 s	SH-SY5Y cells	Cancer therapies	101
P3HT	Thin films, nanoparticles	532–587	20	60 s	HL-1 murine cardiac muscle cells	Tissue engineering	37
P3HT:PCBM	Thin films	561	0.7–13	—	Rat neocortical astrocytes	Cellular physiology	35
P3HT:PCBM	Thin films	532	10	20 ms	Hippocampal neurons	Neural tissue engineering	32
P3HT, P3HT:PCBM	Thin films	510–550	15–30	500 ms	Hippocampal neurons, explanted retinas from Royal College of Surgeons (RCS) rats, hippocampal slices	Visual restoration	33
P3HT/graphene	Bilayer films	530	5–50 lux 110 cd m^{-2}	20 s 100 ms	5-month-old RCS rats	Visual restoration	41
P3HT/PEDOT:PSS	Bilayer films	515	1–30 lux 20 cd m^{-2}	2 s 100 ms	Dystrophic RCS rats	Visual restoration	43
Ti/P3HT:PCBM/ PEDOT:PSS	Trilayer films	560	0.047–29.07	10 ms	Retinal explants obtained from retinal degeneration 10 mouse model	Visual restoration	46
P3HT:N2200	Thin films	410, 533, 575	0.01–0.6	200 ms	Explanted early-stage chick retina	Visual restoration	45
P3HT:Bebq2	Thin films	532	—	—	hiPSC-derived retinal ganglion cells	Visual restoration	48
P3HT	Micro/nanostructured films	470	1.5–46.5	5 ms	HEK-293 cells	Biomedical devices	47
P3HT	Nanofibrils, nanorods	539	0.07	1 s	hfNSCs	Neurogenesis	61
P3HT	Microfibres, nanofibers	623	28.8	30 min	PC12 cells	Neural tissue engineering	62
P3HT/Gel/ PLA-*co*-PCL	Core@shell nanofibers	421–670	1.7 W	1 h	ASCs	Skin tissue engineering	97
P3HT/HDPE	Micropatterned films	530	40	200 ms	C2C12 cells	Tissue regeneration	56
P3HT-*g*-PLA	Porous films	520	110	2.5 s	HUVECs	ROS modulation in vascular tissue	57
P3HT	Nanoparticles	White light	0.06, 0.124	8 h	*Hydra vulgaris*	Tissue regeneration	102
P3HT	Nanoparticles	530	0.43	1–4 min	*Hydra vulgaris*	Visual restoration	131
P3HT	Nanoparticles	540	40	500 ms	Retinal ganglion cells, blind rat retinal explants	Visual restoration	80
P3HT	Nanoparticles	530 400–700	20 lux 0.175	20 s 100 ms	Pupillary reflex rat model Aged retinas rat model	Visual restoration	94
P3HT	Nanoparticles	530	20	200 ms	Rodent model of retinitis pigmentosa (RCS rats)	Visual restoration	87
P3HT-NHS	Nanoparticles	550	207	20 ms, 200 ms	HEK293T cells	Cell membrane polarization	74
P3HT@PTDO	Core@shell nanoparticles	530 White light	0.67 0.124	5 min 4 h, 24 h	HEK293T cells *Hydra vulgaris* model	ROS therapies	77
P3HT-*g*-PLA	Porous nanoparticles	530	0.06	200 ms	HUVECs	ROS modulation in vascular tissue	79

new class of polythiophene-based polymers was synthesized, with oligoethylene glycol side chains that improve water stabilization during electrochemical doping.[120–122] Additionally, such polymers exhibit a huge volumetric change accompanied by a change in the mechanical properties of the film during electrochemical doping, which can be modulated by either the applied voltage, the side chain symmetry, or the ionic strength of the electrolyte.[123,124] Finally, these glycolated polymers are among the first conducting polymers hitting the MPa modulus range already in the pristine state, favouring a better match between cells and material. The intimate interface between the polymer and the cells is responsible for the adhesion between both, which determines the good capability of the polymer to actuate the desired modulation. However, such an interface is another point in bioelectronics, as polymers detach from the destination tissue, or even from electrodes during recording. To solve this problem, thiophene-based trimers with water solubility have been proposed (Fig. 9A).[125] The trimer structure is composed of an ''active'' molecule, in the central part, and two polymerizable units on the two sides, sharing a covalent bond. The polymerization takes place on the side units, without affecting the physicochemical properties of the central part. Such trimers show a lower polymerization energy with respect to single thiophene monomers, as well as water solubility. Similar trimers with alternating EDOT:polythiophene structures have also been reported.[125] The polymerization of these trimers *in vivo* was carried out by Stavrinidou and co-workers in living plant roots (Fig. 4B). The polymerization was promoted by H_2O_2, as the naturally occurring levels of H_2O_2 in plants are high enough to promote entire root encapsulation.[126–128] The concentration of hydrogen peroxide in plants is higher than that of mammalian cells; hence further optimization of the system was proposed to translate such an approach to mammalian cells. A similar trimer was used for *in situ* polymerization in living zebrafish and food samples, with the help of peroxidase enzymes to increase the local H_2O_2 concentration and start the oxidative polymerization.[129] Such *in vivo* polymerized electrodes can potentially allow for *in vivo* and *in situ* formation of electrodes, proposing a whole new, substrate-free direction in organic bioelectronics.

6. Conclusions and outlook

This review article provided a comprehensive overview of the employment of P3HT-based materials for cutting-edge (bio-opto)electronic applications. Different physical and chemical strategies were adopted to engineer P3HT-based materials with different morphologies, mainly in the form of nanoparticles and films with different structures, and advanced functional properties, which guided their final applications. Nevertheless, the additive manufacturing of P3HT-based materials has not yet been explored, opening new possibilities and applications in the future. Taking advantage of the biocompatibility of P3HT and its dual optical and conductive properties, it is used in a wide variety of (bio-opto)electronic applications. A summary of the main works referenced in this review article, which reported the development of different types of P3HT-based materials from their synthesis to their photo-stimulation treatment for a wide range of biomedical applications, is provided in Table 1. Most applications of P3HT-based materials were focused on photostimulation therapies for neuromodulation and regenerative medicine due to the excellent sensitivity of P3HT to visible light. However, their employment for biosensing purposes, where only conductivity plays a key role and the optical properties are not required, was less explored, probably because of the lower electronic conductivity of P3HT in comparison with PEDOT. Concerning future perspectives in this field, a new class of polythiophene-based polymers was recently reported to design materials with enhanced interface properties for better integration with the biological components (*e.g.*, cells, tissues, organs). To that aim, trimers based on thiophene are gaining growing interest as they can be polymerized in water. In addition, this polymerization takes place only on the side units, without affecting the physicochemical properties of the central part, which portrays a field with a huge number of possibilities for the next generation of (bio-opto)electronic materials and devices. It is noteworthy that although P3HT is a promising material for (bio-opto)electronic applications, its direct involvement in clinical trials is still limited, and further research is necessary.

Data availability

No primary research results, software or code have been included and no new data were generated or analysed as part of this review.

Conflicts of interest

There are no conflicts to declare.

Acknowledgements

This work received funding from European Union's Horizon 2020 research and innovation programme under the Marie Sklodowska-Curie grant agreement No. 101034379, and the European Research Council (ERC) under the European Union's Horizon 2020 research and innovation program ''LINCE'' under Grant Agreement 803621. M.C.-G. thanks ''Ayuda RYC2022-036380-I financiada por MICIU/AEI/10.13039/501100011033 y por el FSE+'' and the Emakiker program of POLYMAT (UPV/EHU).

References

1 S. Garg and N. Goel, *J. Phys. Chem. C*, 2022, **126**, 9313–9323.
2 B. Ding, V. Le, H. Yu, G. Wu, A. V. Marsh, E. Gutiérrez-Fernández, N. Ramos, M. Rimmele, J. Martín, J. Nelson, A. F. Paterson and M. Heeney, *Adv. Electron. Mater.*, 2024, **10**, 2300580.

3 M. Criado-Gonzalez, A. Dominguez-Alfaro, N. Lopez-Larrea, N. Alegret and D. Mecerreyes, *ACS Appl. Polym. Mater.*, 2021, **3**, 2865–2883.
4 Y. Jiang and K. Pu, *Acc. Chem. Res.*, 2018, **51**, 1840–1849.
5 D. Gao, K. Parida and P. S. Lee, *Adv. Funct. Mater.*, 2020, **30**, 1907184.
6 Y. Liu, V. R. Feig and Z. Bao, *Adv. Healthcare Mater.*, 2021, **10**, 2001916.
7 P. Sista, K. Ghosh, J. S. Martinez and R. C. Rocha, *J. Nanosci. Nanotechnol.*, 2014, **14**, 250–272.
8 B. de Boer and A. Facchetti, *Polym. Rev.*, 2008, **48**, 423–431.
9 M. J. Donahue, A. Sanchez-Sanchez, S. Inal, J. Qu, R. M. Owens, D. Mecerreyes, G. G. Malliaras and D. C. Martin, *Mater. Sci. Eng., R*, 2020, **140**, 100546.
10 A. A. Gharia, C. J. Bradfield, E. P. W. Jenkins, I. D. C. Fraser and G. G. Malliaras, *Sci. Adv.*, 2024, **10**, eado5042.
11 C. Barberio, J. Saez, A. Withers, M. Nair, F. Tamagnini and R. M. Owens, *Adv. Healthcare Mater.*, 2022, **11**, 2200941.
12 Z. Ali, M. Hassan Sayyad and A. Ali, *Mater. Sci. Eng., B*, 2024, **304**, 117391.
13 N. Yaghoobi Nia, M. Bonomo, M. Zendehdel, E. Lamanna, M. M. H. Desoky, B. Paci, F. Zurlo, A. Generosi, C. Barolo, G. Viscardi, P. Quagliotto and A. Di Carlo, *ACS Sustainable Chem. Eng.*, 2021, **9**, 5061–5073.
14 W. T. Choi and A. J. Bard, *J. Phys. Chem. C*, 2020, **124**, 3439–3447.
15 J. Hynynen, D. Kiefer, L. Yu, R. Kroon, R. Munir, A. Amassian, M. Kemerink and C. Müller, *Macromolecules*, 2017, **50**, 8140–8148.
16 D. Neusser, C. Malacrida, M. Kern, Y. M. Gross, J. van Slageren and S. Ludwigs, *Chem. Mater.*, 2020, **32**, 6003–6013.
17 H. Maddali, K. L. House, T. J. Emge and D. M. O'Carroll, *RSC Adv.*, 2020, **10**, 21454–21463.
18 B. O'Connor, E. P. Chan, C. Chan, B. R. Conrad, L. J. Richter, R. J. Kline, M. Heeney, I. McCulloch, C. L. Soles and D. M. DeLongchamp, *ACS Nano*, 2010, **4**, 7538–7544.
19 R. Giridharagopal, L. Q. Flagg, J. S. Harrison, M. E. Ziffer, J. Onorato, C. K. Luscombe and D. S. Ginger, *Nat. Mater.*, 2017, **16**, 737–742.
20 Y. Zhong, V. Untilova, D. Muller, S. Guchait, C. Kiefer, L. Herrmann, N. Zimmermann, M. Brosset, T. Heiser and M. Brinkmann, *Adv. Funct. Mater.*, 2022, **32**, 2202075.
21 C. G. Bischak, L. Q. Flagg, K. Yan, T. Rehman, D. W. Davies, R. J. Quezada, J. W. Onorato, C. K. Luscombe, Y. Diao, C.-Z. Li and D. S. Ginger, *J. Am. Chem. Soc.*, 2020, **142**, 7434–7442.
22 S. Bellani, D. Fazzi, P. Bruno, E. Giussani, E. V. Canesi, G. Lanzani and M. R. Antognazza, *J. Phys. Chem. C*, 2014, **118**, 6291–6299.
23 E. Mosconi, P. Salvatori, M. I. Saba, A. Mattoni, S. Bellani, F. Bruni, B. Santiago Gonzalez, M. R. Antognazza, S. Brovelli, G. Lanzani, H. Li, J.-L. Brédas and F. De Angelis, *ACS Energy Lett.*, 2016, **1**, 454–463.
24 H. Sies and D. P. Jones, *Nat. Rev. Mol. Cell Biol.*, 2020, **21**, 363–383.
25 H. Shinohara and H. Nishide, *MRS Commun.*, 2024, **14**, 281–286.
26 S. Bellani, A. Ghadirzadeh, L. Meda, A. Savoini, A. Tacca, G. Marra, R. Meira, J. Morgado, F. Di Fonzo and M. R. Antognazza, *Adv. Funct. Mater.*, 2015, **25**, 4531–4538.
27 I. Abdel Aziz, M. Malferrari, F. Roggiani, G. Tullii, S. Rapino and M. R. Antognazza, *iScience*, 2020, **23**, 101091.
28 N. Martino, P. Feyen, M. Porro, C. Bossio, E. Zucchetti, D. Ghezzi, F. Benfenati, G. Lanzani and M. R. Antognazza, *Sci. Rep.*, 2015, **5**, 8911.
29 G. Scarpa, A.-L. Idzko, S. Götz and S. Thalhammer, *Macromol. Biosci.*, 2010, **10**, 378–383.
30 G. Scarpa, A. L. Idzko, A. Yadav, E. Martin and S. Thalhammer, *IEEE Trans. Nanotechnol.*, 2010, **9**, 527–532.
31 F. Lodola, N. Martino, G. Tullii, G. Lanzani and M. R. Antognazza, *Sci. Rep.*, 2017, **7**, 8477.
32 D. Ghezzi, M. R. Antognazza, M. Dal Maschio, E. Lanzarini, F. Benfenati and G. Lanzani, *Nat. Commun.*, 2011, **2**, 166.
33 P. Feyen, E. Colombo, D. Endeman, M. Nova, L. Laudato, N. Martino, M. R. Antognazza, G. Lanzani, F. Benfenati and D. Ghezzi, *Sci. Rep.*, 2016, **6**, 22718.
34 D. Ghezzi, M. R. Antognazza, R. Maccarone, S. Bellani, E. Lanzarini, N. Martino, M. Mete, G. Pertile, S. Bisti, G. Lanzani and F. Benfenati, *Nat. Photonics*, 2013, **7**, 400–406.
35 V. Benfenati, N. Martino, M. R. Antognazza, A. Pistone, S. Toffanin, S. Ferroni, G. Lanzani and M. Muccini, *Adv. Healthcare Mater.*, 2014, **3**, 392–399.
36 F. Lodola, V. Vurro, S. Crasto, E. Di Pasquale and G. Lanzani, *Adv. Healthcare Mater.*, 2019, **8**, 1900198.
37 M. Malferrari, G. Tullii, C. Ronchi, C. Marzuoli, I. A. Aziz, M. R. Antognazza and S. Rapino, *Electrochim. Acta*, 2023, **457**, 142429.
38 E. Šafaříková, L. Švihálková Šindlerová, S. Stříteský, L. Kubala, M. Vala, M. Weiter and J. Víteček, *Sens. Actuators, B*, 2018, **260**, 418–425.
39 F. Lodola, V. Rosti, G. Tullii, A. Desii, L. Tapella, P. Catarsi, D. Lim, F. Moccia and M. R. Antognazza, *Sci. Adv.*, 2019, **5**, eaav4620.
40 S. Negri, P. Faris, G. Tullii, M. Vismara, A. F. Pellegata, F. Lodola, G. Guidetti, V. Rosti, M. R. Antognazza and F. Moccia, *Cell Calcium*, 2022, **101**, 102502.
41 S. Francia, S. Di Marco, M. L. DiFrancesco, D. V. Ferrari, D. Shmal, A. Cavalli, G. Pertile, M. Attanasio, J. F. Maya-Vetencourt, G. Manfredi, G. Lanzani, F. Benfenati and E. Colombo, *Adv. Mater. Technol.*, 2023, **8**, 2201467.
42 M. R. Antognazza, M. Di Paolo, D. Ghezzi, M. Mete, S. Di Marco, J. F. Maya-Vetencourt, R. Maccarone, A. Desii, F. Di Fonzo, M. Bramini, A. Russo, L. Laudato, I. Donelli, M. Cilli, G. Freddi, G. Pertile, G. Lanzani, S. Bisti and F. Benfenati, *Adv. Healthcare Mater.*, 2016, **5**, 2271–2282.
43 J. F. Maya-Vetencourt, D. Ghezzi, M. R. Antognazza, E. Colombo, M. Mete, P. Feyen, A. Desii, A. Buschiazzo, M. Di Paolo, S. Di Marco, F. Ticconi, L. Emionite, D. Shmal, C. Marini, I. Donelli, G. Freddi, R. Maccarone, S. Bisti, G. Sambuceti, G. Pertile, G. Lanzani and F. Benfenati, *Nat. Mater.*, 2017, **16**, 681–689.

44 S. Vaquero, C. Bossio, S. Bellani, N. Martino, E. Zucchetti, G. Lanzani and M. R. Antognazza, *J. Mater. Chem. B*, 2016, **4**, 5272–5283.
45 V. Gautam, D. Rand, Y. Hanein and K. S. Narayan, *Adv. Mater.*, 2014, **26**, 1751–1756.
46 L. Ferlauto, M. J. I. Airaghi Leccardi, N. A. L. Chenais, S. C. A. Gilliéron, P. Vagni, M. Bevilacqua, T. J. Wolfensberger, K. Sivula and D. Ghezzi, *Nat. Commun.*, 2018, **9**, 992.
47 G. Tullii, A. Desii, C. Bossio, S. Bellani, M. Colombo, N. Martino, M. R. Antognazza and G. Lanzani, *Org. Electron.*, 2017, **46**, 88–98.
48 C.-C. Hsu, Y.-Y. Lin, T.-C. Yang, A. A. Yarmishyn, T.-W. Lin, Y.-L. Chang, D.-K. Hwang, C.-Y. Wang, Y.-Y. Liu, W.-L. Lo, C.-H. Peng, S.-J. Chen and Y.-P. Yang, *Int. J. Mol. Sci.*, 2019, **20**, 2661.
49 C.-Y. Li, G.-H. Jiang, T. Higashihara and Y.-C. Lin, *ACS Appl. Mater. Interfaces*, 2024, **16**, 52753–52765.
50 Y. Peng, L. Gao, C. Liu, J. Deng, M. Xie, L. Bai, G. Wang, Y. Cheng, W. Huang and J. Yu, *Nano Res.*, 2023, **16**, 10206–10214.
51 S. Yu, J. K. Harris and E. L. Ratcliff, *ACS Appl. Electron. Mater.*, 2024, **6**, 3127–3137.
52 J. Harris, M. Brothers, V. Coyle, S. Kim and E. Ratcliff, *Chem. Mater.*, 2024, **36**, 324–331.
53 A. Mariano, C. Lubrano, U. Bruno, C. Ausilio, N. B. Dinger and F. Santoro, *Chem. Rev.*, 2022, **122**, 4552–4580.
54 G. Tullii, S. Donini, C. Bossio, F. Lodola, M. Pasini, E. Parisini, F. Galeotti and M. R. Antognazza, *ACS Appl. Mater. Interfaces*, 2020, **12**, 5437–5446.
55 G. Tullii, F. Giona, F. Lodola, S. Bonfadini, C. Bossio, S. Varo, A. Desii, L. Criante, C. Sala, M. Pasini, C. Verpelli, F. Galeotti and M. R. Antognazza, *ACS Appl. Mater. Interfaces*, 2019, **11**, 28125–28137.
56 V. Vurro, A. D. Scaccabarozzi, F. Lodola, F. Storti, F. Marangi, A. M. Ross, G. M. Paternò, F. Scotognella, L. Criante, M. Caironi and G. Lanzani, *Adv. Photonics Res.*, 2021, **2**, 2000103.
57 M. Criado-Gonzalez, L. Bondi, C. Marzuoli, E. Gutierrez-Fernandez, G. Tullii, C. Ronchi, E. Gabirondo, H. Sardon, S. Rapino, M. Malferrari, T. Cramer, M. R. Antognazza and D. Mecerreyes, *ACS Appl. Mater. Interfaces*, 2023, **15**, 35973–35985.
58 C. Liu, J. Deng, L. Gao, J. Cheng, Y. Peng, H. Zeng, W. Huang, L.-W. Feng and J. Yu, *Adv. Electron. Mater.*, 2023, **9**, 2300119.
59 R. Wei, M. Gryszel, L. Migliaccio and E. D. Głowacki, *J. Mater. Chem. C*, 2020, **8**, 10897–10906.
60 A. D. Batista, W. Renzi, R. V. Fernandes, E. Laureto, J. L. Duarte and H. de Santana, *J. Electron. Mater.*, 2019, **48**, 6008–6017.
61 K. Yang, J. Y. Oh, J. S. Lee, Y. Jin, G.-E. Chang, S. S. Chae, E. Cheong and H. K. Baik, *Theranostics*, 2017, **7**, 4591–4604.
62 Y. Wu, Y. Peng, H. Bohra, J. Zou, V. D. Ranjan, Y. Zhang, Q. Zhang and M. Wang, *ACS Appl. Mater. Interfaces*, 2019, **11**, 4833–4841.
63 M.-F. Lin, K.-W. Chang, C.-H. Lee, X.-X. Wu and Y.-C. Huang, *Sci. Rep.*, 2022, **12**, 14842.
64 M. Mbarek, M. Ltayef, M. Almoneef and K. Alimi, *Polym. Eng. Sci.*, 2025, **65**, 1416–1423.
65 N. E. Persson, P.-H. Chu, M. McBride, M. Grover and E. Reichmanis, *Acc. Chem. Res.*, 2017, **50**, 932–942.
66 A. Holmes, E. Deniau, C. Lartigau-Dagron, A. Bousquet, S. Chambon and N. P. Holmes, *ACS Nano*, 2021, **15**, 3927–3959.
67 F. Di Maria, F. Lodola, E. Zucchetti, F. Benfenati and G. Lanzani, *Chem. Soc. Rev.*, 2018, **47**, 4757–4780.
68 F. Di Maria, A. Zanelli, A. Liscio, A. Kovtun, E. Salatelli, R. Mazzaro, V. Morandi, G. Bergamini, A. Shaffer and S. Rozen, *ACS Nano*, 2017, **11**, 1991–1999.
69 E. Zucchetti, M. Zangoli, I. Bargigia, C. Bossio, F. Di Maria, G. Barbarella, C. D'Andrea, G. Lanzani and M. R. Antognazza, *J. Mater. Chem. B*, 2017, **5**, 565–574.
70 C. Bossio, I. Abdel Aziz, G. Tullii, E. Zucchetti, D. Debellis, M. Zangoli, F. Di Maria, G. Lanzani and M. R. Antognazza, *Front. Bioeng. Biotechnol.*, 2018, **6**, 114.
71 S. T. Kim, K. Saha, C. Kim and V. M. Rotello, *Acc. Chem. Res.*, 2013, **46**, 681–691.
72 P. Howes, M. Green, J. Levitt, K. Suhling and M. Hughes, *J. Am. Chem. Soc.*, 2010, **132**, 3989–3996.
73 L. P. Fernando, P. K. Kandel, P. C. Ackroyd and K. A. Christensen, *Anal. Bioanal. Chem.*, 2012, **404**, 3003–3014.
74 M. Zangoli, F. Di Maria, E. Zucchetti, C. Bossio, M. R. Antognazza, G. Lanzani, R. Mazzaro, F. Corticelli, M. Baroncini and G. Barbarella, *Nanoscale*, 2017, **9**, 9202–9209.
75 C. Xing, L. Liu, H. Tang, X. Feng, Q. Yang, S. Wang and G. C. Bazan, *Adv. Funct. Mater.*, 2011, **21**, 4058–4067.
76 E. Miceli, M. Kar and M. Calderón, *J. Mater. Chem. B*, 2017, **5**, 4393–4405.
77 M. Zangoli, A. Cantelli, A. Candini, A. Lewinska, F. Fardella, A. Tino, G. Tommasini, M. Wnuk, M. Moschetta, S. Perotto, M. Lucarini, C. Tortiglione, G. Lanzani and F. Di Maria, *J. Phys. Chem. C*, 2023, **127**, 4672–4683.
78 P. Beer, P. M. Reichstein, K. Schötz, D. Raithel, M. Thelakkat, J. Köhler, F. Panzer and R. Hildner, *J. Phys. Chem. A*, 2021, **125**, 10165–10173.
79 M. Criado-Gonzalez, C. Marzuoli, L. Bondi, E. Gutierrez-Fernandez, G. Tullii, P. Lagonegro, O. Sanz, T. Cramer, M. R. Antognazza and D. Mecerreyes, *Nano Lett.*, 2024, **24**, 7244–7251.
80 J. F. Maya-Vetencourt, G. Manfredi, M. Mete, E. Colombo, M. Bramini, S. Di Marco, D. Shmal, G. Mantero, M. Dipalo, A. Rocchi, M. L. DiFrancesco, E. D. Papaleo, A. Russo, J. Barsotti, C. Eleftheriou, F. Di Maria, V. Cossu, F. Piazza, L. Emionite, F. Ticconi, C. Marini, G. Sambuceti, G. Pertile, G. Lanzani and F. Benfenati, *Nat. Nanotechnol.*, 2020, **15**, 698–708.
81 F. Monti, G. Manfredi, I. E. Palamà, A. Kovtun, M. Zangoli, S. D'Amone, L. Ortolani, G. Bondelli, T. Szreder, K. Bobrowski, M. D'Angelantonio, G. Lanzani and F. Di Maria, *Adv. Healthcare Mater.*, 2021, **10**, 2001306.
82 Y. Sun, H. Li, Y. Lin, L. Niu and Q. Wang, *RSC Adv.*, 2016, **6**, 72519–72524.

83 A. Subramanian, U. M. Krishnan and S. Sethuraman, *BioMed Res. Int.*, 2013, **2013**, 390518.
84 H.-H. Chou, A. Nguyen, A. Chortos, J. W. F. To, C. Lu, J. Mei, T. Kurosawa, W.-G. Bae, J. B. H. Tok and Z. Bao, *Nat. Commun.*, 2015, **6**, 8011.
85 H. J. Son, S. Jeong, I. Jeong, H.-J. Kim and M. Park, *ACS Appl. Nano Mater.*, 2022, **5**, 13027–13036.
86 M. Berggren, E. D. Głowacki, D. T. Simon, E. Stavrinidou and K. Tybrandt, *Chem. Rev.*, 2022, **122**, 4826–4846.
87 G. Chiaravalli, T. Ravasenga, E. Colombo, S. Francia, S. Di Marco, R. Sacco, G. Pertile, F. Benfenati and G. Lanzani, *Phys. Chem. Chem. Phys.*, 2024, **26**, 47–56.
88 J. Hopkins, L. Travaglini, A. Lauto, T. Cramer, B. Fraboni, J. Seidel and D. Mawad, *Adv. Mater. Technol.*, 2019, **4**, 1800744.
89 D. Zhao, R. Huang, J.-M. Gan and Q.-D. Shen, *ACS Nano*, 2022, **16**, 19892–19912.
90 E. Joseph, M. Ciocca, H. Wu, S. Marcozzi, M. A. Ucci, K. Keremane, L. Zheng, B. Poudel, C. Wu, A. Camaioni, K. Wang, S. Priya and T. M. Brown, *npj Biosensing*, 2024, **1**, 15.
91 A. Savva, A. Hama, G. Herrera-López, T. Schmidt, L. Migliaccio, N. Steiner, M. Kawan, H. Fiumelli, P. J. Magistretti, I. McCulloch, D. Baran, N. Gasparini, R. Schindl, E. D. Głowacki and S. Inal, *Adv. Sci.*, 2023, **10**, 2300473.
92 M. J. I. Airaghi Leccardi, N. A. L. Chenais, L. Ferlauto, M. Kawecki, E. G. Zollinger and D. Ghezzi, *Commun. Mater.*, 2020, **1**, 21.
93 P. Vagni, M. J. I. Airaghi Leccardi, C.-H. Vila, E. G. Zollinger, G. Sherafatipour, T. J. Wolfensberger and D. Ghezzi, *Nat. Commun.*, 2022, **13**, 3678.
94 S. Francia, D. Shmal, S. Di Marco, G. Chiaravalli, J. F. Maya-Vetencourt, G. Mantero, C. Michetti, S. Cupini, G. Manfredi, M. L. DiFrancesco, A. Rocchi, S. Perotto, M. Attanasio, R. Sacco, S. Bisti, M. Mete, G. Pertile, G. Lanzani, E. Colombo and F. Benfenati, *Nat. Commun.*, 2022, **13**, 3677.
95 B. Huang, X. Liu and D. Xing, *Eur. Polym. J.*, 2024, **213**, 113096.
96 M. Zangoli and F. Di Maria, *View*, 2021, **2**, 20200086.
97 G. Jin, M. P. Prabhakaran and S. Ramakrishna, *Photochem. Photobiol.*, 2014, **90**, 673–681.
98 S. Negri, P. Faris, R. Berra-Romani, G. Guerra and F. Moccia, *Front. Phys.*, 2020, **10**, 1618.
99 I. A. Aziz and M. R. Antognazza, *MRS Adv.*, 2020, **5**, 3473–3489.
100 I. Abdel Aziz, L. Maver, C. Giannasi, S. Niada, A. T. Brini and M. R. Antognazza, *J. Mater. Chem. C*, 2022, **10**, 9823–9833.
101 M. Ciocca, S. Marcozzi, P. Mariani, V. Lacconi, A. Di Carlo, L. Cinà, M. D. Rosato-Siri, A. Zanon, G. Cattelan, E. Avancini, P. Lugli, S. Priya, A. Camaioni and T. M. Brown, *Adv. NanoBiomed Res.*, 2023, **3**, 2200127.
102 G. Onorato, F. Fardella, A. Lewinska, F. Gobbo, G. Tommasini, M. Wnuk, A. Tino, M. Moros, M. R. Antognazza and C. Tortiglione, *Adv. Healthcare Mater.*, 2022, **11**, 2200366.
103 F. Milos, G. Tullii, F. Gobbo, F. Lodola, F. Galeotti, C. Verpelli, D. Mayer, V. Maybeck, A. Offenhäusser and M. R. Antognazza, *ACS Appl. Mater. Interfaces*, 2021, **13**, 23438–23451.
104 M. Moros, A. Lewinska, G. Onorato, M. R. Antognazza, M. Di Francesca, M. Blasio, G. Lanzani, A. Tino, M. Wnuk and C. Tortiglione, *MRS Commun.*, 2018, **8**, 918–925.
105 Y.-S. Hsiao, Y.-H. Liao, H.-L. Chen, P. Chen and F.-C. Chen, *ACS Appl. Mater. Interfaces*, 2016, **8**, 9275–9284.
106 S. Gáspár, T. Ravasenga, R.-E. Munteanu, S. David, F. Benfenati and E. Colombo, *Materials*, 2021, **14**, 4761.
107 B. Yuan, M. R. F. Aziz, S. Li, J. Wu, D. Li and R.-K. Li, *Acta Biomater.*, 2022, **139**, 82–90.
108 C. Wu, Y. Pu, Y. Zhang, X. Liu, Z. Qiao, N. Xin, T. Zhou, S. Chen, M. Zeng, J. Tang, J. Pi, D. Wei, J. Sun, F. Luo and H. Fan, *Adv. Healthcare Mater.*, 2022, **11**, 2201255.
109 E. Macchia, D. Alberga, K. Manoli, G. F. Mangiatordi, M. Magliulo, G. Palazzo, F. Giordano, G. Lattanzi and L. Torsi, *Sci. Rep.*, 2016, **6**, 28085.
110 M. C. Sportelli, R. A. Picca, K. Manoli, M. Re, E. Pesce, L. Tapfer, C. Di Franco, N. Cioffi and L. Torsi, *Appl. Surf. Sci.*, 2017, **420**, 313–322.
111 D. Blasi, F. Viola, F. Modena, A. Luukkonen, E. Macchia, R. A. Picca, Z. Gounani, A. Tewari, R. Österbacka, M. Caironi, Z. M. Kovacs Vajna, G. Scamarcio, F. Torricelli and L. Torsi, *J. Mater. Chem. C*, 2020, **8**, 15312–15321.
112 N. Elnagar, N. Elgiddawy, W. M. A. El Rouby, A. A. Farghali and H. Korri-Youssoufi, *Anal. Lett.*, 2024, 1–23.
113 Z. Meng, Y. Zhang, L. Yang, S. Zhao, Q. Zhou, J. Chen, J. Sui, J. Wang, L. Guo, L. Chang, J. He, G. Wang and G. Zang, *Research*, 2023, **6**, 0149.
114 S. Liu, Y. Fu, G. Li, L. Li, H. K.-W. Law, X. Chen and F. Yan, *Adv. Mater.*, 2017, **29**, 1701733.
115 C.-J. Lim, S. Lee, J.-H. Kim, H.-J. Kil, Y.-C. Kim and J.-W. Park, *ACS Appl. Mater. Interfaces*, 2018, **10**, 41026–41034.
116 S.-Y. Yu, T.-W. Tung, H.-Y. Yang, G.-Y. Chen, C.-C. Shih, Y.-C. Lee, C.-C. Chen, H.-W. Zan, H.-F. Meng, C.-J. Lu, C.-L. Wang, W.-B. Jian and O. Soppera, *ACS Sens.*, 2019, **4**, 1023–1031.
117 Z. Wang, R. Ruan, G. Lin, S. He, Y. Liu, C. Gong, P. Xiao, J. Chen, Y. Lu, Y. Cao, X. Lin and J. Zhang, *Chem. Eng. J.*, 2023, **468**, 143603.
118 F. Benfenati and G. Lanzani, *Nat. Rev. Mater.*, 2021, **6**, 1–4.
119 D. Wood, I. Hancox, T. S. Jones and N. R. Wilson, *J. Phys. Chem. C*, 2015, **119**, 11459–11467.
120 J. Gladisch, E. Stavrinidou, S. Ghosh, A. Giovannitti, M. Moser, I. Zozoulenko, I. McCulloch and M. Berggren, *Adv. Sci.*, 2020, **7**, 1901144.
121 M. Moser, T. C. Hidalgo, J. Surgailis, J. Gladisch, S. Ghosh, R. Sheelamanthula, Q. Thiburce, A. Giovannitti, A. Salleo, N. Gasparini, A. Wadsworth, I. Zozoulenko, M. Berggren, E. Stavrinidou, S. Inal and I. McCulloch, *Adv. Mater.*, 2020, **32**, 2002748.
122 S. Zokaei, D. Kim, E. Järsvall, A. M. Fenton, A. R. Weisen, S. Hultmark, P. H. Nguyen, A. M. Matheson, A. Lund, R. Kroon, M. L. Chabinyc, E. D. Gomez, I. Zozoulenko and C. Müller, *Mater. Horiz.*, 2022, **9**, 433–443.

123 I. Abdel Aziz, J. Gladisch, C. Musumeci, M. Moser, S. Griggs, C. J. Kousseff, M. Berggren, I. McCulloch and E. Stavrinidou, *Mater. Horiz.*, 2024, **11**, 2021–2031.
124 I. Abdel Aziz, J. Gladisch, S. Griggs, M. Moser, H. Biesmans, A. Beloqui, I. McCulloch, M. Berggren and E. Stavrinidou, *J. Mater. Chem. B*, 2024, **12**, 4029–4038.
125 L. Vallan, E. Istif, I. J. Gómez, N. Alegret and D. Mantione, *Polymers*, 2021, **13**, 1977.
126 D. Mantione, E. Istif, G. Dufil, L. Vallan, D. Parker, C. Brochon, E. Cloutet, G. Hadziioannou, M. Berggren, E. Stavrinidou and E. Pavlopoulou, *ACS Appl. Electron. Mater.*, 2020, **2**, 4065–4071.
127 G. Dufil, D. Parker, J. Y. Gerasimov, T.-Q. Nguyen, M. Berggren and E. Stavrinidou, *J. Mater. Chem. B*, 2020, **8**, 4221–4227.
128 D. Parker, Y. Daguerre, G. Dufil, D. Mantione, E. Solano, E. Cloutet, G. Hadziioannou, T. Näsholm, M. Berggren, E. Pavlopoulou and E. Stavrinidou, *Mater. Horiz.*, 2021, **8**, 3295–3305.
129 X. Strakosas, H. Biesmans, T. Abrahamsson, K. Hellman, M. S. Ejneby, M. J. Donahue, P. Ekström, F. Ek, M. Savvakis, M. Hjort, D. Bliman, M. Linares, C. Lindholm, E. Stavrinidou, J. Y. Gerasimov, D. T. Simon, R. Olsson and M. Berggren, *Science*, 2023, **379**, 795–802.
130 L. Bondi, C. Marzuoli, E. Gutiérrez-Fernández, G. Tullii, J. Martín, B. Fraboni, D. Mecerreyes, M. R. Antognazza and T. Cramer, *Adv. Electron. Mater.*, 2023, **9**, 2300146.
131 C. Tortiglione, M. R. Antognazza, A. Tino, C. Bossio, V. Marchesano, A. Bauduin, M. Zangoli, S. V. Morata and G. Lanzani, *Sci. Adv.*, 2017, **3**, e1601699.

